

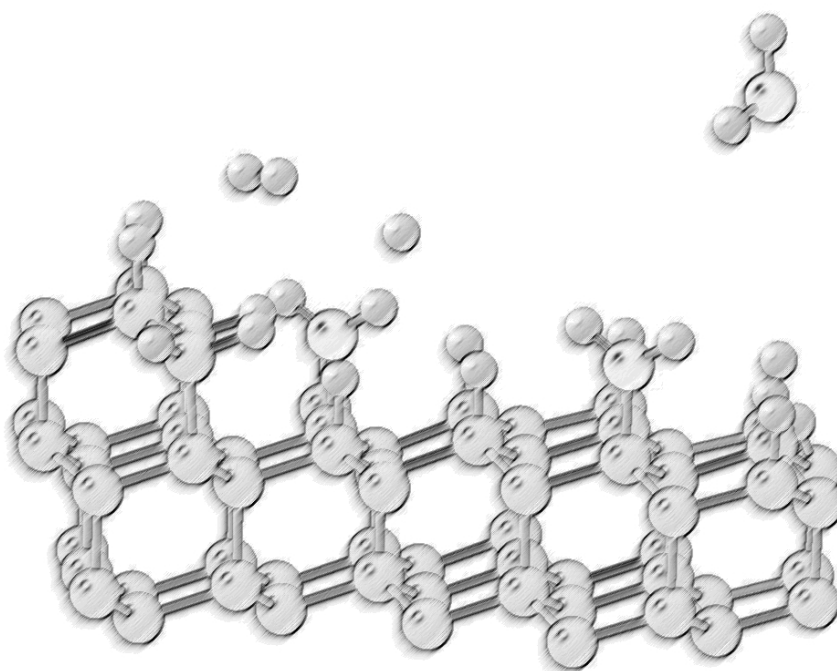
Comprehensive Summaries of Uppsala Dissertations
from the Faculty of Science and Technology 637



Theoretical Modelling of Thin Film Growth in the B-N System

BY

BJÖRN MÅRLID



ACTA UNIVERSITATIS UPSALIENSIS
UPPSALA 2001

Dissertation for the Degree of Doctor of Philosophy in Inorganic Chemistry presented at Uppsala University in 2001

ABSTRACT

Mårlid, B. 2001. Theoretical Modelling of Thin Film Growth in the B-N System. Acta Universitatis Upsaliensis. *Comprehensive Summaries of Uppsala Dissertations from the Faculty of Science and Technology* 637. 64 pp. Uppsala. ISBN 91-554-5048-2.

In vapour phase deposition, the knowledge and control of homogeneous and heterogeneous reactions in connection to precursor design may lead to the deposition of the desired material; structure or phase. This thesis is a document attempting to increase the knowledge of film growth in the B-N system.

In the present work, surface processes like adsorption, abstraction, migration and nucleation have been modelled on an atomic scale using density functional theory (DFT). The systems studied are mainly cubic and hexagonal boron nitride surfaces ((c-BN) vs. (h-BN)), but also the α -boron (001) surface.

It has been shown that DFT and a cluster approach is a reliable tool in modelling boron nitride surfaces and surface processes, provided that certain functionals, basis sets and geometrical constraints are used.

By using surface stabilisers such as H species in an electron- or radical-rich environment, it has been shown that *i*) the structure of cubic boron nitride surfaces can be sustained, and *ii*) c-BN may nucleate on the h-BN (001) basal plane. Furthermore, the nucleation of c-BN from arbitrary and experimental growth species is energetically preferable over a continuous growth of h-BN on the h-BN (001) edges.

An atomic layer deposition (ALD) process for boron nitride was developed. It resulted in turbostratic (t-BN), transparent, well-adherent and almost atomically smooth BN films. However, with the cubic phase of boron nitride absent in the ALD films, more effort needs to be put into both the theoretical and the experimental branches of this field of science.

Key words: Boron nitride, boron, theoretical modelling, DFT, surface processes, surfaces, thin films, growth, ALD.

Björn Mårlid, Department of Materials Chemistry, Ångström Laboratory, Uppsala University, Box 538, SE-751 21 Uppsala, Sweden

© Björn Mårlid 2001

ISSN 1104-232X

ISBN 91-554-5048-2

Printed in Sweden by Eklundshofs Grafiska AB, Uppsala 2001

Till min, och Tildes morfar.

Preface

This thesis comprises the present summary and the following papers. They are referred to in the summary by their Roman numerals.

- I. **Theoretical investigation of hydrogen- and halogen-terminated c-BN (111) clusters**
Björn Mårlid, Karin Larsson and Jan-Otto Carlsson
Phys. Rev. B **60**, 16039 (1999).

- II. **Hydrogen and Fluorine Adsorption on the h-BN (001) Plane**
Björn Mårlid, Karin Larsson and Jan-Otto Carlsson
J. Phys. Chem. B **103**, 7637 (1999).

- III. **Nucleation of c-BN on Hexagonal Boron Nitride**
Björn Mårlid, Karin Larsson and Jan-Otto Carlsson
Accepted for publication in Phys. Rev. B

- IV. **Nucleation of c-BN on h-BN from Experimental Growth Species**
Björn Mårlid, Karin Larsson and Jan-Otto Carlsson
Submitted to J. Phys. Chem. B

- V. **Chemical Interaction of H₂, Br₂ and HBr with α -Boron Surfaces**
Björn Mårlid, Karin Larsson and Jan-Otto Carlsson
Submitted to J. Phys. Chem. B

- VI. **Density Functional Methods in BN Surface Modeling**
Björn Mårlid and Karin Larsson
Submitted to Phys. Rev. B

- VII. **Atomic Layer Deposition (ALD) of BN Thin Films**
Björn Mårlid, Mikael Ottosson, Karin Larsson and Jan-Otto Carlsson
Submitted to Thin Solid Films

CONTENTS

1. INTRODUCTION.....	7
1.1. Boron Nitride Phases.....	7
1.2. Properties and Applications of Boron Nitride.....	9
1.3. BN Thin Film Deposition.....	9
2. DENSITY FUNCTIONAL THEORY (DFT).....	13
2.1. Introduction.....	13
2.2. Hohenberg-Kohn Theorems.....	14
2.3. Local Density Methods.....	16
2.4. Gradient Corrected Methods.....	17
2.5. Hybrid Methods.....	19
3. DFT RELIABILITY IN BORON NITRIDE MODELLING.....	21
3.1. Introduction.....	21
3.2. Choice of Functionals.....	21
3.3. Basis Sets Effects.....	24
3.4. Size Effects.....	27
4. RESULTS.....	29
4.1. Cubic BN (111) Clusters.....	29
4.2. Cubic BN (111) Surfaces.....	33
4.3. Nucleation on h-BN.....	35
4.4. Boron deposition.....	44
5. ALD OF BORON NITRIDE.....	49
5.1. Introduction.....	49
5.2. Atomic Layer Deposition (ALD).....	49
5.3. Experimental details and results.....	51
6. CONCLUDING REMARKS.....	55
7. ACKNOWLEDGEMENT.....	57
REFERENCES.....	59

1. INTRODUCTION

1.1. Boron Nitride Phases

General

The elements boron (group III) and nitrogen (group V), both neighbours to carbon (group IV) in the Periodic Table, form 1:1 compounds, which are isostructural and isoelectronic to the polymorphs of carbon. The hexagonal modification of boron nitride (h-BN) has a layered sp^2 -bonded structure similar to graphite (Fig. 1),¹ and it is sometimes called “white graphite”. Hexagonal BN was prepared for the first time in the mid-19th century.^{2,3} It remained a laboratory curiosity for more than hundred years, until hot-pressed h-BN shapes were firstly made in 1957.⁴ Hexagonal boron nitride is the only BN phase found in nature. The cubic modification (c-BN) is a hard sp^3 -bonded diamond-like phase with a cubic zincblende structure (Fig. 1).¹ In 1957, cubic BN was first grown in bulk crystalline form by using a high pressure and high temperature method.⁵ Reports of c-BN thin films, deposited by high-frequency reactive sputtering appeared as early as 1970.⁶ However, it was not until 1987 that thin films prepared by a physical vapour deposition (PVD) method (activated reactive evaporation) were conclusively characterised as c-BN.⁷ Hexagonal and cubic BN are the only two stable phases of boron nitride. The stacking sequences in h-BN and c-BN can vary, producing also metastable sp^2 - and sp^3 -bonded polytypes (Fig. 1.1). By rearranging the basal planes of sp^2 -bonded BN in a staggered arrangement, rhombohedral BN (r-BN) is obtained. The metastable sp^3 -bonded modification of boron nitride is wurtzitic BN (w-BN), which is analogous to hexagonal diamond.¹

As with graphitic carbon, sp^2 -bonded boron nitride is often found in a disordered, turbostratic form (t-BN). This is the form of sp^2 -bonded material most commonly observed in boron nitride thin films. For a turbostratic structure, the two-dimensional in-plane order of hexagonal basal planes is largely retained, but these planes are stacked in a random sequence and with random rotation around the c-axis.⁸ Thin films of boron nitride may also be formed without a distinct crystallographic order and without any distinctly identified phase. The films are then defined as amorphous boron nitride (a-BN).

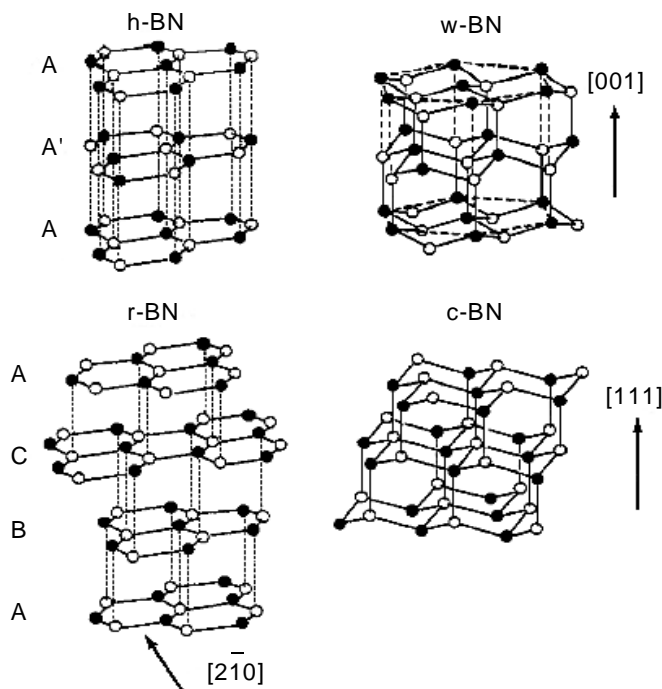


Figure 1.1. Structures of the sp^2 -bonded phases h-BN and r-BN, and the sp^3 -bonded phases w-BN and c-BN.

Phase stability

Cubic boron nitride is commercially synthesised in bulk form by the application of high pressures and temperatures (HP-HT). The original development of the pressure-temperature (P - T) phase diagram⁹ indicated that h-BN is thermodynamically stable at ambient temperatures and pressures, whereas c-BN is only stable at high temperatures. This is in analogy to the diamond-graphite P - T phase diagram. However, recent experiments and calculations suggest that the P - T phase boundary line should be shifted to lower pressures, which would make c-BN stable under ambient conditions.¹⁰⁻¹³ Regardless of the exact position of the phase boundary line, a significant kinetic barrier hinders the direct transition of bulk material from sp^2 - to sp^3 -hybridisation under ambient conditions.

1.2. Properties and Applications of Boron Nitride

Hexagonal boron nitride is widely used because of its combination of properties, e.g., low density, high temperature stability, chemical inertness, stability in air up to 1000°C, stability to thermal shock, easy workability of hot-pressed shapes, excellent electrical insulating character, very high thermal conductivity.^{1,14} Bulk h-BN can therefore be used as a solid lubricant and as a ceramic insulating material in high-temperature environments. It can also be employed as a crucible for melting glass and metals, and as a neutron absorber and shield for nuclear reactors. Thin films of h-BN have potential applications to semiconductors as a protective coating, as a gate insulator in a metal-insulator-semiconductor field-effect transistor (MISFET), as a diffusion source, and as a thin film varistor or voltage limiter. Boron nitride films can also be used as transparent substrates for X-ray lithography masks, and as protective coatings.^{15,16}

Cubic boron nitride has a number of extreme and highly desirable mechanical, thermal, electrical, and optical properties.^{1,17} Cubic BN has a Vickers hardness of about 4500 kg mm⁻², which makes it second in hardness only to diamond, and, hence, it is a natural candidate for hard, protective coatings.¹⁷ The fact that c-BN *i*) does not react readily with ferrous metals (as does diamond)¹⁸, and *ii*) has a high resistance to oxidation (at temperatures as high as 1300°C) makes it even more attractive compared to diamond for tooling applications or as an abrasive.¹⁷ Cubic BN is transparent in the infrared (IR) and near ultraviolet (UV) parts of the spectrum, and thus is sought after as a protective coating for IR and UV optics.¹⁴ Because of its wide bandgap ($E_g \approx 6$ eV) and good thermal conductivity, c-BN can be used in high-power microwave and millimetre wave devices. Furthermore, cubic boron nitride can more easily than diamond be doped both p- and n-type to make p-n junction diodes which can work at high temperatures.¹

1.3. BN Thin Film Deposition

The deposition methods of BN films can be separated into either of two routes; the “physical” and the “chemical” one.¹⁹ Until now it has only been possible to achieve nanocrystalline c-BN layers via the physical route, i.e., via physical vapour deposition (PVD). The PVD methods comprise for example rf and magnetron sputtering from B and BN targets, ion-beam-assisted deposition (IBAD) in connection with laser ablation or an electron beam, and ion beam deposition with B⁺ and N⁺.^{20,21} However, the PVD BN films suffer from poor adhesion to almost any substrate material, limiting the maximum film thickness to a few hundred nanometers only. Two reasons are generally responsible for the poor adhesion. Firstly, the strong ion bombardment, which seems to be necessary to obtain the cubic modification,²² results in films with a high compressive stress. Secondly, the structure of PVD films most often follows the widely accepted model of a layered growth.^{23,24}

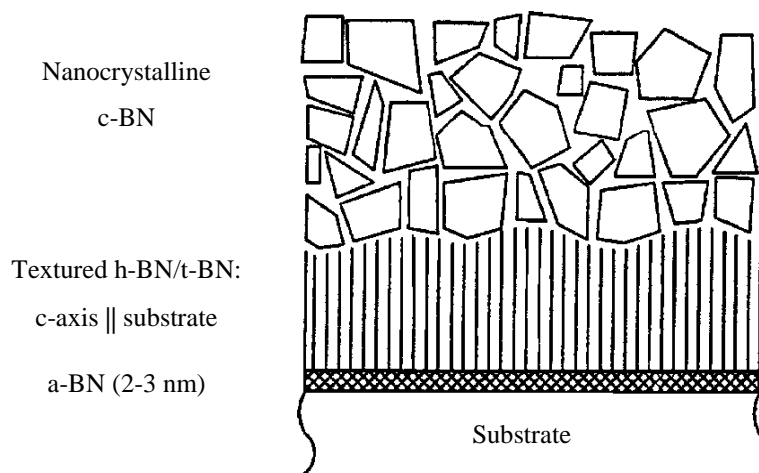


Figure 1.2. Schematic presentation of the structure of most PVD deposited BN films (from Ref. [28]).

The three-layered film is a consequence of the nucleation of c-BN, which generally does not occur directly on the substrate, but rather in the sequence; a-BN \rightarrow textured h-BN/t-BN \rightarrow nanocrystalline c-BN (Fig. 1.2). The mechanically weak h-BN/t-BN interlayer may then cause the films to delaminate. Furthermore, the grain boundaries in the c-BN layer consist of poorly crystallised sp^2 -bonded BN,^{23,25} which is easily attacked by air moisture to form boric acid and consequently soften.²⁶ The c-BN grains may then peel off from the substrate.²⁷

Whereas the physical route implies brute force by ion bombardment, the chemical route represents a more gentle deposition process. Chemical vapour deposition (CVD) is the material synthesis method in which a mixture of gaseous reactants is transported in the vapour phase to a heated substrate surface. Chemical reactions, or pyrolysis, then occur on the surface to form a solid film deposit. The chemical route comprises thermally activated (TACVD), hot-filament-assisted (HF-CVD), atomic layer (ALCVD) and plasma-enhanced (PECVD) chemical vapour deposition methods. The conditions during a CVD process are often close to equilibrium and films containing less defects may therefore be deposited. Thus, a successful CVD process for c-BN is likely to yield high quality films. Unfortunately, the CVD films have so far mostly consisted of a multiphase mixture of amorphous, turbostratic and hexagonal boron nitride.^{16,29,30} However, a PECVD deposition of boron nitride from a single-source boron- and nitrogen- containing precursor borane-ammonia (H_3BNH_3) have lately showed evidence of various proportions of c-BN in a sp^2 -bonded matrix.³¹

It can thus be concluded that BN films deposited from either of the two routes, physical or chemical, are *i*) of insufficient quality, or, *ii*) of the undesired BN phase (sp^2 -bonded). While experimental studies of the nucleation and growth of c-BN by ion-assisted deposition methods (following the physical route) have proven successful,^{20,21,27,32-35} the fundamental understanding of such processes is still rather poor. Several theoretical and experimental studies, comparing the deposition of diamond and c-BN, have been presented from a thermodynamic point of view.^{29,36,37} Furthermore, the nucleation of boron nitride on nickel substrates,³⁸ as well as the role of gas-phase reactions in BN CVD, have also been investigated.³⁹⁻⁴¹ However, at least to my knowledge, it has not lead to the development of a successful CVD deposition method for c-BN.

So in the search, documented in this thesis, for a deeper and more fruitful knowledge at an atomic level, the density functional theory (DFT) has been used to investigate the surface termination, nucleation and growth process of boron nitride films. The knowledge acquired may then be employed in precursor design for a successful deposition of cubic boron nitride by means of CVD. After this brief introduction to the B-N system and a short review of the current status of BN deposition, a summary of DFT will follow in chapter 2. The reliability of DFT as a tool for modelling BN surface processes (**papers III** and **VI**) is presented in chapter 3 (i.e., the effect of functionals, basis set, and model size on structural and energetic parameters). This is in chapter 4 followed by the main results of **papers I - V**; surface termination of c-BN (111) clusters and c-BN (111) surfaces, nucleation of c-BN on the basal plane and basal plane edges, respectively, of h-BN, and, finally, the chemical interaction of gaseous H_2 , Br_2 and HBr with α -B (001) surfaces. Chapter 5 is devoted to the experimental part of the investigations (**paper VII**). The Atomic Layer Deposition (ALD) method and the ALD reactor design are there briefly discussed, together with the results from the deposition experiments.

2. DENSITY FUNCTIONAL THEORY (DFT)

2.1. Introduction

Over the last five-ten years Density Functional Theory (DFT) has become the most often used approach in computational chemistry for the study of ground state molecular properties. Furthermore, Walter Kohn was 1998 rewarded the Nobel Prize for the development of density functional methods. What makes DFT such a successful computational method?

Thanks to the introduction of the direct methodology by Almlöf et al.,¹ it is now possible to do large Hartree-Fock Self-Consistent-Field (HF-SCF) calculations with a fairly good basis set. The computational cost scales as N^4 , with N being the number of electrons.

The Hartree-Fock theory is based on Schrödinger's time-independent equation ($\hat{H}\Psi = E\Psi$), where E is the electronic energy, $\Psi = \Psi(\mathbf{x}_1, \mathbf{x}_2, \dots, \mathbf{x}_n)$ is the wave function, and \hat{H} is the Hamiltonian operator, $\hat{H} = \hat{T} + \hat{V}_{ne} + \hat{V}_{ee}$. \hat{T} is the kinetic operator, \hat{V}_{ne} is the electron-nucleus attraction operator, and \hat{V}_{ee} is the electron-electron repulsion energy operator. The Hartree approximation in HF may also be called the "mean-field" approximation, since each of the electrons interact with the average potential created by all the other electrons of the system. Furthermore, in HF, the wave function Ψ is approximated as an antisymmetrised product of N orthonormal spin orbitals ($\phi_i(\mathbf{x})$), the Slater determinant. However, the exact wave function for a many-electron system is not a single determinant. The above approximations in HF theory will lead to an error in the calculated energy, called *correlation energy* (E_{corr}^{HF}).

$$E_{corr}^{HF} = E - E_{HF} \quad (2.1)$$

To account for the correlation energy, one must go beyond the HF-SCF level. This will then imply difficulties, which are associated with the accurate representation of the electron-electron cusp. The problem is that this convergence is very slow² and correlated calculations and large basis sets are required in order to achieve "chemical accuracy" (± 1 kcal/mol). The different methods for correlation treatment are Møller-Plesset perturbation theory (MP2, 3, 4, etc...), configuration interaction (CI) and coupled cluster (CC) calculations, and the raw computational cost for these correlated methods scales to the power of 5 or more. DFT, on the other hand, can be regarded as an SCF method with correction for the correlation included; yet it scales only to the power of 3 or in practice even near-linear scaling.³

Historically, DFT goes all the way back to the birth of quantum chemistry. Thomas and Fermi stated (1927) that the energy of a system could be calculated as a function of its electron density; $E = f(\rho)$ (see Equation 2.2).⁴⁻⁶ J.C. Slater⁷ suggested in 1951 that the difficult exchange term in the Hartree-Fock method should be replaced by the Dirac⁸ $\rho^{1/3}$ potential, which he argued included both exchange and correlation effects. Two major issues of discouragement then appeared. First, the bond energies of molecules from the original DFT were largely overbound. Second, in 1962, Teller proved that if you calculate the energy as being a function of the electron density no chemical bonds exist.⁹ However, two key theorems produced in 1964 by Hohenberg and Kohn rebutted Teller's criticism and proved the usefulness of DFT.¹⁰

2.2. Hohenberg-Kohn Theorems

The proof by Hohenberg and Kohn¹⁰ simply states that the electron density, $\rho(\mathbf{r})$, determines the ground-state electronic energy, i.e. there exists a one-to-one correspondence between the electron density of a system and the energy. This means that if you know the exact electron density $\rho(\mathbf{r})$, then the cusps of $\rho(\mathbf{r})$ would occur at the positions of the nuclei. Moreover, knowing $|\nabla\rho(\mathbf{r})|$ at the nuclei would give their nuclear charges.¹¹ The original formulation of Hohenberg and Kohn was: *The external potential $v(\mathbf{r})$ is determined, within a trivial additive constant, by the electron density $\rho(\mathbf{r})$.* We have, by writing E_v for E to make explicit the dependence on the specific external potential (“v”);

$$\begin{aligned} E_v[\rho] &= T[\rho] + V_{ne}[\rho] + V_{ee}[\rho] = T[\rho] + \int \rho(\mathbf{r})v(\mathbf{r})d\mathbf{r} + V_{ee}[\rho] = \\ &= T[\rho] + \int \rho(\mathbf{r})v(\mathbf{r})d\mathbf{r} + J[\rho] + E_{xc}[\rho] \end{aligned} \quad (2.2)$$

where $T[\rho]$ represents the kinetic energy, $V_{ne}[\rho]$ is the electron-nucleus interaction energy and $V_{ee}[\rho]$ is the electron-electron interaction energy which contains the classical coulomb interaction energy ($J[\rho]$) and the exchange-correlation energy ($E_{xc}[\rho]$). Thus, by knowing the electron density, ρ , we know the number of electrons, N , the external potential, $v(\mathbf{r})$, and hence all the properties of the ground state. The only problem with the Hohenberg-Kohn theorem is that the functional connecting the electron density and the ground-state energy is not known.¹²

The second theorem of Hohenberg and Kohn provides the energy variational principle, although it restricts the theory to ground states only.. It reads: *For a trial density $\tilde{\rho}(\mathbf{r})$, such that $\tilde{\rho}(\mathbf{r}) \geq 0$ and $\int \tilde{\rho}(\mathbf{r})d\mathbf{r} = N$,*

$$E_0 \leq E_v[\tilde{\rho}] \quad (2.3)$$

where $E_v[\tilde{\rho}]$ is the energy functional of (2.2). This is analogous to the variational principle for wave functions, which states that the energy computed from a guessed wave function, Ψ , is an upper bound to the true ground-state energy, E_0 . The importance of this theorem is its practicality, namely that if we assume that we have a good functional representation, then we can minimise it to get the most accurate orbitals and structure.

Kohn-Sham Orbitals

The basic idea in the Kohn and Sham formalism is the splitting of the kinetic energy functional into two parts. One which can be calculated exactly, and one which constitutes a small correction term. Kohn and Sham¹³ therefore introduced the idea of considering the determinantal wave function for N non-interacting electrons in N orbitals, ϕ_i . For such a system the kinetic energy and the electron density are exactly given as

$$T_s[\rho] = \sum_{i=1}^N \langle \phi_i | -\frac{1}{2}\nabla^2 | \phi_i \rangle \quad (2.4)$$

$$\rho(\mathbf{r}) = \sum_{i=1}^N |\phi_i(\mathbf{r})|^2 \quad (2.5)$$

The subscript S denotes that it is the kinetic energy calculated from a Slater determinant representing a hypothetical system of non-interacting electrons. In a real system the electrons *are* interacting. The remaining kinetic energy, the correction term, is absorbed into an exchange-correlation term. The orbitals, ϕ_i , above obey an equation of the form

$$\left[-\frac{1}{2}\nabla^2 + v_{eff}(\mathbf{r}) \right] \phi_i = \varepsilon_i \phi_i \quad (2.6)$$

The orbital energies ε_i of equation (2.6) can be associated with molecular orbital energies, and the highest occupied orbital energy is the ionisation potential (Koopmans' theorem).¹⁴ However, this is only true if the exact exchange-correlation functional is employed. Since this is not the case in present DFT calculations, the orbital energies of KS equation do not have the same significance as in Hartree-Fock theory.¹⁵ The KS effective potential $v_{eff}(\mathbf{r})$ is defined to include the external potential, the coulomb interaction potential and the exchange-correlation potential.¹² Equation (2.6) can then be rewritten for the non-interacting electrons in N orbitals, which obey the equation

$$\left[-\frac{1}{2}\nabla^2 + v(\mathbf{r}) + \int \frac{\rho(\mathbf{r}')}{|\mathbf{r}-\mathbf{r}'|} d\mathbf{r}' + v_{xc}(\mathbf{r}) \right] \phi_i = \varepsilon_i \phi_i(\mathbf{r}) \quad (2.7)$$

This is the Kohn-Sham equation for the Kohn-Sham orbitals ϕ_i and by identifying the exchange-correlation functional $E_{xc}[\rho]$, equation (2.7) will give the electron density through equation (2.5).

2.3. Local Density Methods

Unlike Hartree-Fock theory, DFT cannot be systematically improved (one of its major drawbacks). While the Kohn-Sham equations exactly incorporate the kinetic energy $T_s[\rho]$, the exchange-correlation functional $E_{xc}[\rho]$ is unsettled. Therefore, the way to deal with the exchange-correlation functional is to start from a model for which there is an exact solution, the uniform electron gas. This is the basic idea behind the *Local Density Approximation* (LDA). The electron density varies slowly on an atomic scale, i.e. the density can locally be treated as a uniform electron gas. The exchange-correlation energy density of each infinitesimal region of the *inhomogeneous* electron distribution, $n(\mathbf{r})$, is then precisely equal to the exchange-correlation energy density of a *homogeneous* electron gas with the same density as the corresponding infinitesimal volume element (Fig. 2.1).

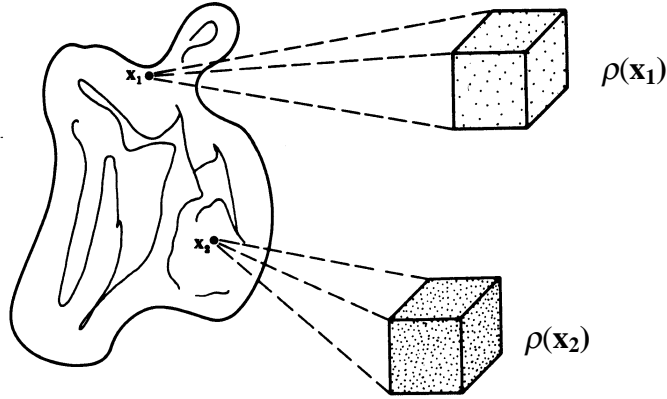


Figure 2.1. Schematic representation of LDA (from Ref. [16]).

By introducing LDA, the exchange-correlation energy can be written as

$$E_{xc}^{LDA}[\rho] = \int \rho(\mathbf{r}) \epsilon_{xc}(\rho) d\mathbf{r} \quad (2.8)$$

where $\epsilon_{xc}(\rho)$ indicates the exchange and correlation energy per particle of a uniform electron gas of density ρ . The function $\epsilon_{xc}(\rho)$ can be divided into one exchange and one correlation term,

$$\epsilon_{xc}(\rho) = \epsilon_x(\rho) + \epsilon_c(\rho) \quad (2.9)$$

The exchange part is known and identified as the Dirac exchange-energy⁸

$$\varepsilon_x(\rho) = -C_x \rho(\mathbf{r})^{1/3}, \quad C_x = 3/4 \left(\frac{3}{\pi} \right)^{1/3} \quad (2.10)$$

In a more general case, where the α and β spin densities are not equal, LDA has been replaced by the *Local Spin Density Approximation* (LSDA). The density ρ above is then the sum of the individual densities, ρ_α and ρ_β .

The correlation energy of the electron gas has been numerically determined by Ceperley and Alder using Monte-Carlo methods for several different densities.¹⁷ By applying a suitable analytic interpolation formula for the high and low density limits, Vosko, Wilk and Nusair (VWN)¹⁸ gave the correlation functional $\varepsilon_c(\rho)$ its accepted form which covers both spin polarised and spin compensated cases.¹⁹

The correct asymptotic behaviour of the exchange-correlation energy, $E_{xc}[\rho]$, goes as r^{-1} . However, the LSDA exchange-correlation energy decays exponentially and, thus, overestimates $E_{xc}[\rho]$, often by a factor of ~ 2 . This in turn leads to overestimated bond dissociation energies and underestimated bond lengths in comparison to experiments.^{20,21} Compared to the Gaussian-2 (G2) test set, LSDA overbinds by 90.9 kcal/mol (G2 is a large test set (148 molecules) of good and credible experimental data).²²

2.4. Gradient Corrected Methods

It is clear that the LSDA is not adequate for useful predictions within computational chemistry. The improvements over LSDA have to consider a non-uniform electron gas. Such methods are known as *Gradient Corrected* or *Generalised Gradient Approximation* (GGA) methods, since they make the exchange-correlation energies not only dependent on the density, ρ , but also on the derivative (gradient) of the density, $\nabla\rho$. The GGA methods are sometimes referred to as non-local methods. However, this is misleading since they depend on ρ and $\nabla\rho$ at a given point, and not on a space volume.

A number of methods have been proposed to modify the LSDA exchange and correlation expressions. Examples of gradient-corrected functionals that have gained importance are Perdew86 (P86)²³ (correlation) and Perdew91 (PW91)²⁴ (exchange and correlation). These functionals do not contain semi-empirical parameters and were derived by Perdew and co-workers from properties of the slowly varying electron gas (the jellium model),¹⁶ which means they may be more suitable for metal clusters or d-element systems.

The Becke Exchange Correction

In 1988 Becke²⁵ proposed a widely used correction to the LSDA exchange energy, which may be regarded as responsible for the wide acceptance of DFT as a reliable tool in quantum chemistry. It has the correct asymptotic r^{-1} behaviour for the exchange-energy density, but not for the potential.²⁶

$$\varepsilon_x^{B88} = \varepsilon_x^{LDA} + \Delta\varepsilon_x^{B88} \quad (2.11)$$

$$\Delta\varepsilon_x^{B88} = -\beta\rho^{1/3} \frac{x^2}{1 + 6\beta x \sinh^{-1} x}, \quad x = \frac{|\nabla\rho|}{\rho^{4/3}} \quad (2.12)$$

The β parameter is determined in a way that the sum of the LDA and Becke exchange terms accurately reproduce the exchange energies for the six noble gas atoms ($\beta = 0.0042$). The Becke exchange correction is almost exclusively used in all studies comprised in this thesis. However, in **paper VI** it has been used in comparison with other GGA:s, as well as local functionals.

The Lee-Yang-Parr Correlation Functional

Various gradient-corrected functionals have been proposed for the correlation energy, of which P86 and PW91 are already mentioned (see above). However, these functionals are derived from the electron gas. Instead Colle and Salvetti²⁷ presented an approximate correlation energy formula for helium in terms of the second-order Hartree-Fock density matrix. Lee, Yang and Parr (LYP)²⁸ then turned this formula into an explicit functional of ρ . The LYP functional contains gradient terms and the great advantage of this is that it is derived from an actual correlated wave function for a two-electron system, and has no relation to the uniform electron gas.

$$\varepsilon_c^{LYP} = -a \frac{\gamma}{(1 + d\rho^{-1/3})} - ab \frac{\gamma e^{-c\rho^{-1/3}}}{9(1 + d\rho^{-1/3})\rho^{8/3}} \quad (2.13)$$

$$x \left[18(2^{2/3})C_F(\rho_\alpha^{8/3} + \rho_\beta^{8/3}) - 18\rho t_w \right. \\ \left. + \rho_\alpha(2t_w^\alpha + \nabla^2\rho_\alpha) + \rho_\beta(2t_w^\beta + \nabla^2\rho_\beta) \right]$$

where a , b , c and d parameters are determined from the fitting to the data of the helium atom. The t_w functional is known as the local Weizsacker kinetic energy density.

2.5. Hybrid Methods

An important development is the introduction of the *Adiabatic Connection Functionals* (ACF) and involves an integration over the parameter λ which “switches on” the electron-electron interaction.

$$E_{xc} = \int_0^1 \langle \Psi_\lambda | \mathbf{V}_{xc}(\lambda) | \Psi_\lambda \rangle d\lambda \quad (2.14)$$

If \mathbf{V}_{xc} is taken to be linear in λ (a very crude approximation), the integral is then given as the average value of $\lambda = 0$ and $\lambda = 1$.

$$E_{xc} \cong \frac{1}{2} \langle \Psi_0 | \mathbf{V}_{xc}(\mathbf{0}) | \Psi_0 \rangle + \frac{1}{2} \langle \Psi_1 | \mathbf{V}_{xc}(\mathbf{1}) | \Psi_1 \rangle \quad (2.15)$$

In the $\lambda = 0$ limit, the electrons are non-interacting and there is no correlation energy, merely exchange energy. The exchange energy is then exactly given by Hartree-Fock theory. However, for the $\lambda = 1$ limit, the exchange-correlation energy is unknown. Approximating it by the LSDA result, the Becke *Half-and-Half* (H+H) method is defined.²⁹

$$E_{xc}^{H+H} = \frac{1}{2} E_x^{exact} + \frac{1}{2} (E_x^{LSDA} + E_c^{LSDA}) \quad (2.16)$$

Becke has also defined a generalised, experimentally fitted version of the (H+H) method. The so called *Becke 3 parameter functional* (B3), is a combination of LSDA, exact exchange, and a gradient correction term for exchange and correlation.³⁰

$$E_{xc}^{B3} = (1-a) E_x^{LSDA} + a E_x^{exact} + b \Delta E_x^{B88} + E_c^{LSDA} + c \Delta E_c^{GGA} \quad (2.17)$$

3. DFT RELIABILITY IN BORON NITRIDE MODELLING

3.1. Introduction

Various approximations within the density functional theory, DFT, were overviewed in the previous chapter. Before starting a DFT computational study of a material's properties, the effect of some important parameters on these properties have to be elucidated. These parameters include; *i*) functional, *ii*) basis set, *iii*) model size, *iv*) geometry optimisation. The first three choices will explicitly be surveyed for boron nitride modelling in the following sections, whereas the geometry optimisation will not be reported here. Throughout the investigations comprised in the thesis, the program system DMol¹ from Biosym/ Molecular Simulation Technologies of San Diego has been used.

3.2. Choice of Functionals

In the first of the Hohenberg-Kohn theorems, it was stated that there exists a one-to-one correspondence between the electron density of a system and the energy.² The only problem with this theorem is that the exact functional connecting them is not known. Thus, different approximations and assumptions have been made for the different available functionals. The correct choice of functional can be made based on the knowledge of how the different functionals have been derived. Unfortunately, the combination of exchange and correlation functional that will be the most reliable for the specific system of interest can be difficult to predict in advance.

In **paper VI**, eight different functionals were investigated regarding their ability to accurately model BN surfaces (h-BN (001)) and BN surface processes (ammonia adsorption on h-BN). Four methods were based on the *local-density approximation* (LDA). They are; *i*) the Kohn-Sham exchange only functional (**KS**),³ *ii*) the Janak-Moruzzi-Williams correlation functional (**JMW**),⁴⁻⁶ *iii*) the Vosko-Wilks-Nusair correlation functional (**VWN**),⁷ and *iv*) the Perdew-Wang local correlation functional (**PWC**).⁸ The last three functionals (JMW, VWN and PWC) are all combined with the Dirac exchange functional.⁹

The other four methods were based on the *generalised gradient approximation* (GGA) and are different combinations of the Becke 1988 exchange functional (B88x),¹⁰ the Lee-Yang-Parr correlation functional (LYPc),¹¹ and the Perdew-Wang 1991

exchange and correlation functionals (PW_X^{GGA} and PW_C^{GGA}).¹² They are then combined to give; *i*) **BLYP** (B88x-LYPc), *ii*) **BP** (B88x- PW_C^{GGA}), *iii*) **PW91** (PW_X^{GGA} - PW_C^{GGA}), and *iv*) **VWN-BP**. The last combination, VWN-BP, is the BP functional with the local correlation functional PW_C^{LDA} replaced by the local correlation functional of VWN. A somewhat more elaborate description of the different LDA and GGA functionals is given in **paper VI**.

A good measure of the reliability of any computational method is the ability of the specific method to numerically reproduce experimental values. Thus, the atomisation energy for bulk BN was calculated using the different LDA and GGA functionals. The atomisation energy of any species can be calculated using the following general formula:

$$E_{at}(X_n Y_m) = nE(X) + mE(Y) - E(X_n Y_m) \quad (3.1)$$

where $E(X_n Y_m)$ is the total energy for the molecule or compound, and $E(X)$ and $E(Y)$ are the total energies for the constituting atoms X and Y, respectively. The results for the atomisation energy are presented in Fig. 3.1, and for comparison, a staggered line representing the experimental value of 4.00 eV¹³ is also present in the figure.

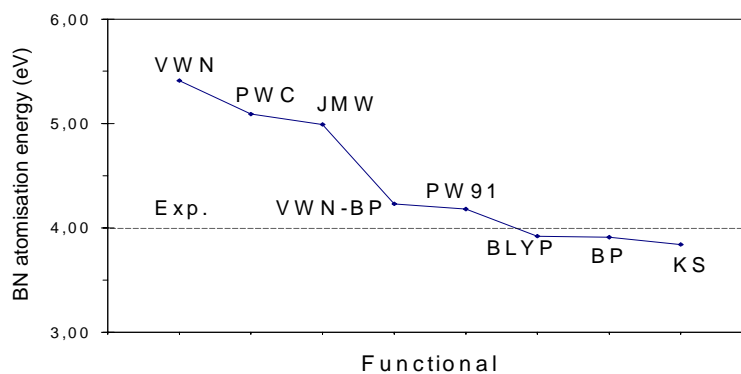


Figure 3.1. Calculated atomisation energy for bulk BN, using different LDA and GGA functionals.

It can be seen that the LDA functionals VWN, PWC and JMW overestimate the atomisation energy and that the introduction of gradient-correction drastically improves the result compared to the experimental value. The average error obtained when using the LDA functionals was 0.91 eV. Surprisingly, the value obtained by the KS functional differs only by 0.16 eV from the experimental value (3.84 vs. 4.00 eV). However, this does not imply that the KS functional is reliable. It is rather that the overbinding of LDA methods is compensated by a very low total energy for BN.

The explanation to this is that the total energies for B and N (using the KS functional) are relatively high compared to the values obtained with the other functionals. From equation (3.1) it can then be seen that this will lead to an atomisation energy that is relatively seen too low. The corresponding average error for the GGA methods was 0.14 eV. The best accuracy compared to experiment was obtained by using the functionals BP and BLYP (3.91 and 3.92 eV, respectively).^{VI}

In BN thin film deposition, one of the most common nitrogen sources is ammonia.¹⁴ Furthermore, sp^2 -hybridised boron nitride is present in both PVD and CVD deposited thin BN films.¹⁴⁻¹⁷ Hence, it would be preferable for the deposition of c-BN to succeed in a continued growth of the cubic phase on a underlying hexagonal phase of h-BN, thereby also suppressing further growth of h-BN. The model system chosen in **paper VI** is therefore the adsorption of NH_3 to the basal plane of h-BN. The obtained adsorption energies for NH_3 on B and N surface sites are presented in Fig. 3.2.

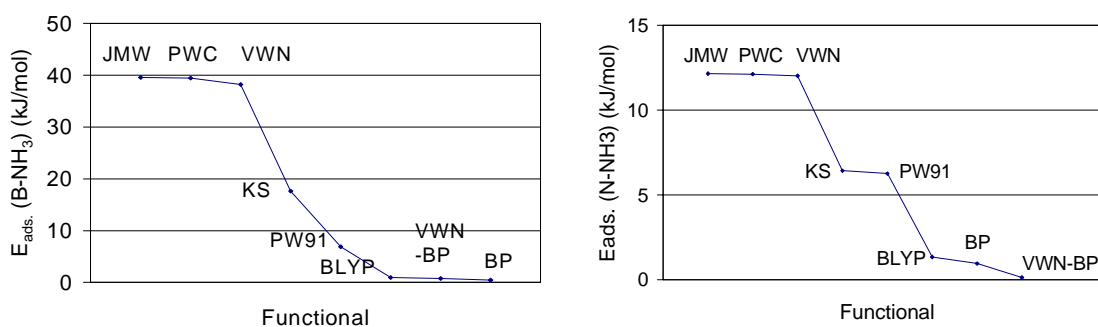


Figure 3.2. Adsorption energy for NH_3 on B (left) and N (right) surface sites of h-BN (001).

Conclusively, it can be seen that the well-known overestimation of bond energies, inherited in the local-density approximation,¹⁸ is present for ammonia adsorption on both B and N sites. Interestingly, the GGA functionals gave adsorption energies that were similar for both sites (B or N) (~1 (for BLYP, BP, VWN-BP), ~6 (for PW91) kJ/mol). Moreover, the adsorption energies obtained with the functionals JMW, VWN and PWC are regardless of adsorption site (B or N), a factor two larger than the results obtained with KS. Furthermore, the results calculated with BLYP, BP and VWN-BP functionals are a factor six less compared to PW91, also regardless of adsorption site. Based on the results of the calculated atomisation energies, the most reliable values of adsorption energy for ammonia on h-BN (001) are probably obtained by the BP and BLYP functionals.

Since BLYP, BP and VWN-BP all include the Becke 1988 gradient-corrected exchange functional (B88x),¹⁰ it appears that the exchange functional plays a more important role for the adsorption energy of this system than does the correlation

functional. The functionals BP, VWN-BP and PW91 all include the same correlation functional derived by Perdew and Wang,⁷ and yet they do not give similar results. The effect of the Perdew-Wang generalised-gradient correlation correction has been evaluated in another study. There it was concluded that the B88x exchange-only functional gave better results for electron conserving reactions (bond breaking or atomisation) in comparison to B88x-PWc^{GGA} (BP). However, for electron non-conserving processes (such as ionisation), the B88x-PWc combination was superior to B88x (even LSDA performed better than B88x).¹⁹

Different geometrical parameters such as bond lengths within the adsorbate, the bond distance between the substrate and the adsorbate, as well as bond angles within both the substrate and the adsorbate, were also investigated in **paper VI**. It was observed that both the LDA methods and the GGA methods resulted in bond lengths for ammonia that were somewhat too long compared to the experimental value²⁰ (by 0.036 Å (LDA) and 0.028 Å (GGA)). Too long predictions of bond lengths is also the general trend for DFT calculations.^{18,21,22} The numerical values obtained for the \angle HNH bond angle of ammonia were, regardless of LDA or GGA method, too large compared to experimental data, whereas the h-BN \angle BNB bond angle was accurately predicted (120°). However, even though the ammonia molecule was found to be only weakly physisorbed to h-BN (001), the bonding of NH₃ to a substrate may still affect the \angle HNH angle to adapt a more “ammonium ion-like” value. The experimental \angle HNH bond angle is 102.3° for ammonia, and 109.5° for the ammonium ion.²⁰

It can then be concluded that the best overall reliability of the LDA and GGA functionals in modelling the BN surfaces (h-BN (001)) and the BN surface processes (ammonia adsorption) was the BLYP functional, closely followed by BP.

3.3. Basis Set Effects

The Hamiltonian operator (i.e., the functionals) does not alone determine the accuracy of a calculation. Also the type of wave function (basis set) will affect the final result. The introduction of basis sets is one of the approximations inherent in *ab initio* methods. The unknown molecular orbitals (MO) are expanded in a set of known functions (basis functions) through the MO=LCAO scheme (*Linear Combination of Atomic Orbitals*). As long as the basis is complete it does not imply an approximation. However, a complete basis set is an infinite number of functions, and it is practically impossible for any calculation. Using pseudopotentials, the basis set generally consists of Gaussian or Slater-type orbitals (GTO, STO) for cluster calculations, whereas plane waves (PW) generally are used for bulk calculations with periodic boundary conditions. The program system DMol uses numerical MO basis sets for the calculations,²³ whereas other *ab initio* programs mostly use analytical ones.

Numerical basis functions are described as values on an atomic-centred spherical-polar mesh. This has the consequence that bonds can undergo exact dissociation and that the basis-set superposition error (BSSE)^{24,25} should be reduced. Furthermore, a good description of weak bonds, like hydrogen bonds, is expected. In earlier investigations of hydrogen-bonded systems, it was found that LDA methods generally fail to reproduce the hydrogen-bond properties, whereas the GGA methods describe the hydrogen bond well.^{22,26,27} The particular type of numerical basis set used in DMol is suggested to be the most efficient for fast-convergent 3-dimensional numerical integration.¹ Four different basis sets were used in **paper VI**. The minimal (min) and double numeric (dn) basis sets uses 1 and 2 atomic orbitals (AO), respectively for each occupied orbital in the free atom. In the double numeric polarisation d-functions (dnd) basis set, polarisation functions are added only to atoms heavier than hydrogen, whereas in the double numeric polarisation (dnp) basis set, polarisation p-functions are also added to hydrogen atoms. The sizes of the dnd and dnp basis sets are comparable to the analytical split-valence polarised basis sets 6-31G* (or DZVP) and 6-31G** (or DZVPP), respectively.^{28,29}

The atomisation energies of bulk BN and gaseous NH₃ were calculated to test the reliability of the basis sets. However, since bulk BN does not contain hydrogen atoms, and the dnd and dnp basis sets differ by the addition of polarisation p-functions to H atoms, the atomisation energy of gaseous NH₃ was also calculated. Gaseous ammonia has an experimental atomisation energy of 4.34±0.07 eV.³⁰ Based on the results for the different functionals, the BLYP gradient-corrected functional was used for both bulk BN and gaseous NH₃. It was found that by using the dnd and dnp basis sets, the calculated numerical values of atomisation energies were closer to the experimental ones (Fig. 3.3). For comparison, the experimental values are added in the figure (as staggered lines).

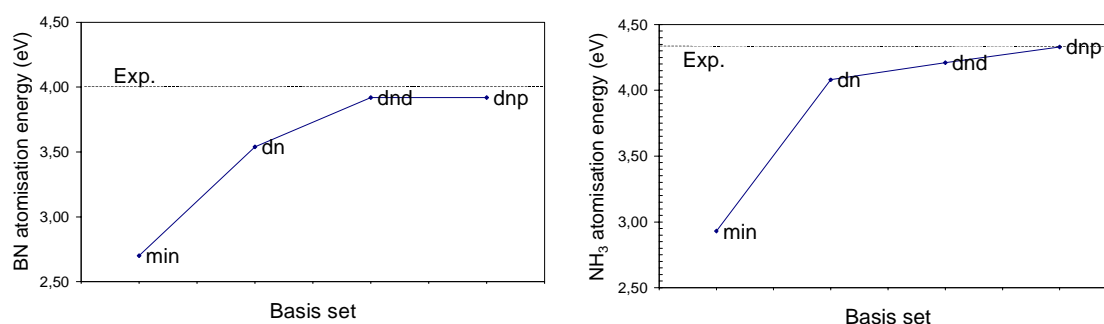


Figure 3.3. Calculated atomisation energy for bulk BN (left) and gaseous NH₃ (right) using different basis sets.

The influence of the differently sized basis sets on NH_3 adsorption onto the basal plane of h-BN was also investigated in **paper VI**. It could be observed that the minimal basis set gave the poorest results for the adsorption energy. Using the dn basis set, the accuracy was dramatically increased and, with the addition of polarisation functions, the adsorption energy for NH_3 was further improved. It was also observed that the adsorption energy was almost identical for both B- and N-sites (Fig. 3.4). The various geometrical parameters, measured to investigate the accuracy of the functionals, were also used to study the influence of different basis sets. The correlation between adsorption energy and the bond distance between the NH_3 adsorbate and the surface, observed for the different functionals used, was also obtained using different basis sets. The shortest bond distance (B- NH_3 or N- NH_3) was calculated using the minimal basis set (~ 3.0 Å), and it also resulted in the highest adsorption energy on both types of surfaces (~ 36 vs. ~ 21 kJ/mol). The other extreme was represented by the most extensive basis set, dnp, which resulted in the longest surface-adsorbate bond distances (4.1 vs. 4.5 Å) and the smallest corresponding adsorption energies (1.0 vs. 1.3 kJ/mol).

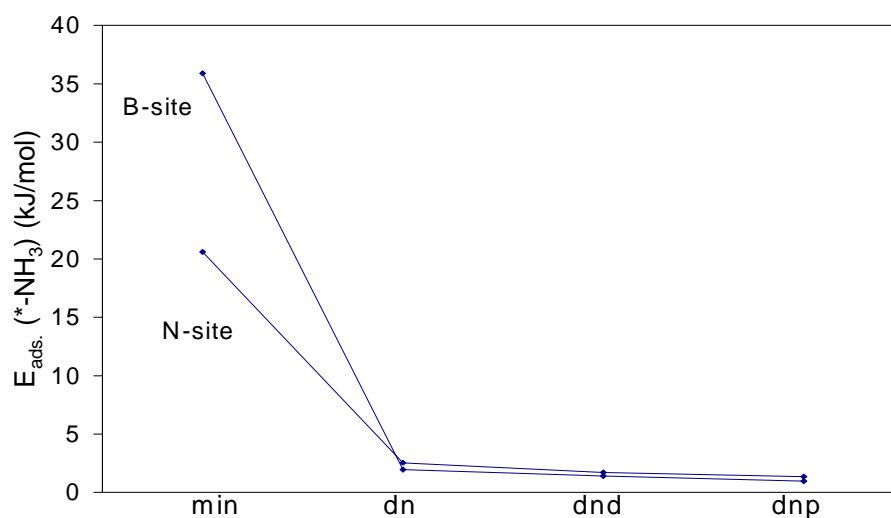


Figure 3.4. Calculated adsorption energy for NH_3 on B- and N surface sites of h-BN (001), using different basis sets.

For the angle $\angle\text{HNN}$ in NH_3 , the minimal basis set showed almost similar values compared to dnd and dnp, whereas the dn basis set deviates by more than 12° from any of the other values. As a result of the geometry optimisation, the ammonia molecule was, using the dn basis set, physisorbed on the h-BN basal plane in an almost flat trigonal structure. On the contrary, the geometry optimisation resulted in the common tetrahedral structure for ammonia when using the other basis sets studied in **paper VI** (min, dnd, and dnp).

It has been reported that there is a fundamental difference between DFT and Hartree-Fock (HF) theory in the response to basis set incompleteness,³¹ and that polarisation functions does not play the same important role in DFT once the basis set has reached a certain size. For example, the DZP basis set (comparable to dnd in DMol) has been found to give satisfying binding energies.³² The introduction of gradient-correction ($\nabla\rho$) is more important than the introduction of polarisation functions, which also has been observed here for BN surface adsorption.

3.4. Size Effects

There are two major approaches to model a realistic crystalline surface, namely as a two-dimensional slab with periodic boundary conditions or as an isolated cluster. Both methods are subjected to certain approximations, and the choice favouring any of them is a question of computational cost and accuracy. Upon reducing the dimensionality and/or the size of the template, quantum effects may appear for some types of materials. The quantum effects are only expected for semiconducting materials with a sufficiently small bandgap, e.g. for Cd_3As_2 with a bandgap of 0.13 eV.³³ Even though BN has an optical bandgap of 5.2 eV (h-BN)³⁴ or 6.4 eV (c-BN),³⁵ minor quantum effects may still be present for very small cluster sizes. Furthermore, these small clusters also have a large number of terminating species (H atoms) compared to the number of B and N atoms. Hence, adsorption energies and geometrical parameters may be affected by edge effects.

In **paper III** the influence of different surface modelling was explicitly investigated using the adsorption of gaseous H to various dimensions of the h-BN basal plane edges as a model. The levels of theory used were the gradient-corrected PW91 for closed-shell systems, and the spin unrestricted variety of PW91 for radical systems.³⁶ The periodic calculations were performed using a different DFT program package, CASTEP from Biosym/ Molecular Simulation Technologies of San Diego, for which the functionals BLYP and BP have not been implemented (only LDA by Perdew-Zunger and GGA by Perdew-Wang (PW91))^{36,37}.

Three different models were used in **paper III**. The largest one is a 2-dimensional slab, which is extended infinitely in one direction (x-axis). It is modelled by a unit cell that is translated in the x-, y- and z-direction during the calculation. Each unit cell contains one layer of eight B_3N_3 -rings fused together and terminated with hydrogen atoms in the third direction (z-axis) (Fig. 3.5 (a)). The medium-sized model is also a 2-dimensional slab extended infinitesimally in one direction. The only difference is that this unit cell contains one layer of *four* B_3N_3 -rings fused together (instead of eight) (Fig. 3.5 (b)). The smallest model in **paper III** is a 3-dimensional cluster of four aligned B_3N_3 -rings terminated with H atoms (Fig. 3.5 (c)). It should be stressed that the three models do not only represent different sizes, they also represent a successively increased ratio of terminating species

(compared to the number of B and N atoms) when going from the larger to the smaller model. The adsorbed hydrogen atom and the edge atom bonding to it were, for all models used, allowed to fully relax during the geometry optimisation.

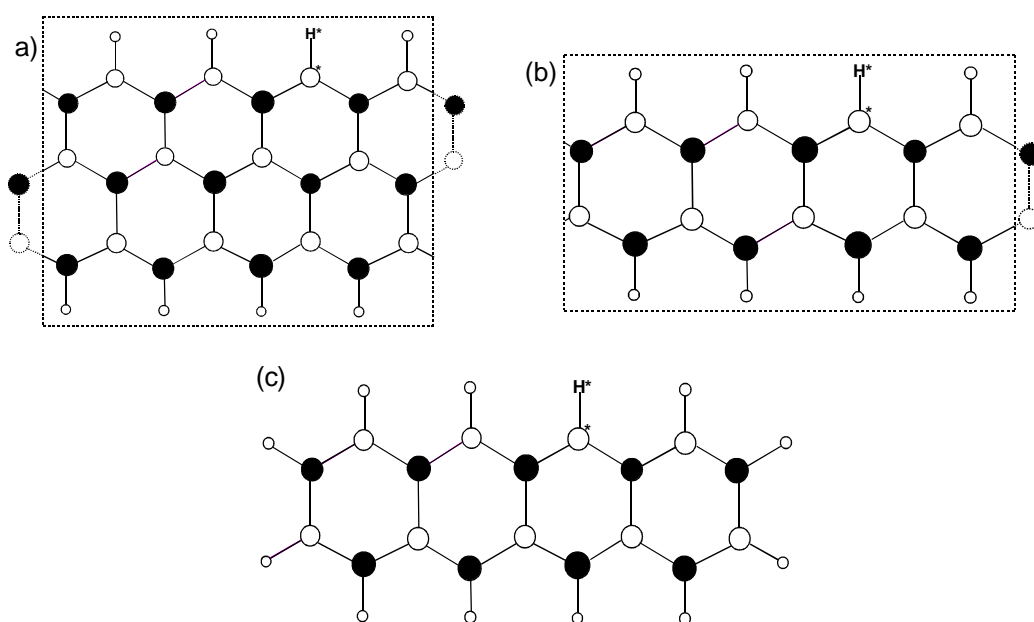


Figure 3.5. An illustration of the (a) large 2-dimensional slab model, (b) small 2-dimensional slab model and (c) cluster model, used in **paper III**. Only the asterisk marked atoms are allowed to relax.

The resulting energies for adsorption of H to the B-rich (100) edge were found to differ by less than about 1 %, upon reducing the dimensionality and size of the model system (as well as changing the H/BN ratio). On the N-rich ($\bar{1}00$) edge, the difference in adsorption energy was somewhat larger than on the (100) edge, but still very small and less than about 2-3 %. It was therefore concluded that the small cluster model is computationally valid in modelling h-BN surfaces and BN surface adsorption. The same conclusion can also be reached regarding H and F adsorption on c-BN (111) surfaces. In **paper I** and Ref. [38], crystalline c-BN (111) surfaces were modelled either as a slab, or as a cluster. The calculated adsorption energies for H and F species were then found to not differ significantly when using either of the models.

To summarise this chapter; BN surface processes like adsorption is adequately and reliably modelled using the gradient-corrected BLYP functional and the dnp basis set. Furthermore, the BN crystalline surfaces may be modelled as clusters provided that adequate constraints are used during the geometry optimisation.

4. RESULTS

The main results of the surface modelling in **papers I – V** will be presented in this chapter. The first two sections will be devoted to cubic boron nitride (111). In section 4.1, the termination of relaxed clusters with a (111) geometry is surveyed. This is followed in section 4.2 by the termination of c-BN (111) surfaces. The nucleation of c-BN is examined in section 4.3, on both the basal plane and the basal plane edges, respectively, of h-BN. Finally, the last section (4.4) summarises the study of the interaction between gaseous H_2 , Br_2 and HBr , respectively, and an α -boron (001) surface.

4.1. Cubic BN (111) Clusters

Introduction

Clusters of different shapes and sizes are often formed (or may be intentionally used) in the gas phase during CVD of thin films. They are also to some extent expected to occur on the growing thin film surface, either because of an adsorption of the gaseous cluster, or as local surface formations obtained at different stages during film growth. These cluster-like particles will then include various numbers of atoms with, hence, a large range of abilities to geometrically relax. The very small clusters will relax more or less totally, while the much larger ones are expected to act more like a crystalline surface.

In diamond CVD, radical hydrogen species are effective in the stabilisation of sp^3 dangling bonds on the growing surface.^{1,2} The question is if surface termination is necessary in sustaining the sp^3 -hybridisation of the surface atoms during c-BN growth. In **paper I**, a small unterminated c-BN cluster (B_7N_6) of the same size as in Fig. 4.1, was allowed to be fully relaxed. A totally collapsed geometrical structure was then obtained. The sp^3 -hybridisation of the original structure was completely converted to sp^2 -hybridisation. Hence, it is obvious that surface termination by a suitable species is of highest importance for a continued growth of cubic boron nitride films. The need for surface termination has earlier been confirmed both theoretically and experimentally.^{3,4} In a molecular dynamics simulation of an unterminated c-BN (111) surface it was stated that the two topmost BN layers are subjected to a graphitisation rather than a reconstruction.³ Thus, the topmost layers are not just flattened out, but also the interlayer distance between the surface layer and the subsurface layer has increased.

In an electron-energy-loss spectroscopy (EELS) study it was observed that cubic BN films exhibited a hexagonal-like top layer with a thickness of about 0.9 nm (~3 monolayers).⁴ The c-BN films were deposited by sputtering of elemental boron under simultaneous bombardment of the substrate with a mixture of argon and nitrogen ions, indicating a low possibility for surface termination of other species than B or N.

sp³ stabilisation

In plasma enhanced (PECVD) and hot-filament (HFCVD) chemical vapour deposition, radical-rich environments are produced. In BN CVD, these environments will include B- and N-containing radical species, as well as hydrogen and halogen ones.

The halogens (especially fluorine) are generally expected to be efficient as surface stabilising agent due to the mono-valent status and highly electronegative value. They will, thus, exhibit a large ability to form strong bonds. Moreover, a hydrogen atom is also effective as a stabilising agent due to its monovalent state and a very small atomic radius. The most obvious choice of surface stabilisers is therefore hydrogen and specific halogens (F, Cl and Br). The heavier halogens are most likely too large, and will thus cause sterical hindrance on the growing surface.

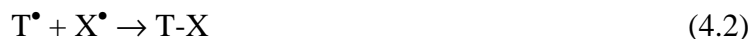
The small B₇N₆H₉X₁₃ (X = H, F, Cl, or Br) cluster shown in Fig. 4.1 has been used in **paper I**. This type of cluster contains several adsorption sites. However, only one is completely and symmetrically surrounded by surface atoms (labelled cB in Fig. 4.1), and was therefore used as a surface site in **paper I**. Since the study aimed at finding stabilisers that would sustain the cubic geometry (sp³-hybridisation) of the cluster atoms, all geometrical parameters were fully relaxed.

The ability of the various terminating species to stabilise the c-BN (111) clusters was determined by different geometric parameters and by the calculated adsorption energy of each species (H, F, Cl, and Br) onto the cluster. Since all atoms in the clusters were allowed to relax during the geometry optimisation, an optimal stabilisation of especially the radical cluster was obtained (leading to a very low E_T). Thus, the numerical value for the adsorption energy, obtained with these types of clusters, can be regarded as a lower limit with respect to corresponding adsorption processes occurring on more realistic ones.

The geometrical parameters included in **paper I** are *i*) the interatomic cB-N (or cN-B) distance (Fig. 4.1), and *ii*) the angles \angle_{NcBN} and \angle_{BcNB} for the adsorption sites B and N, respectively. The calculated numerical values were compared with *i*) the interatomic B-N distance of bulk c-BN (1.57 Å),⁵ and *ii*) the ideal sp³ and sp² angles of 109.5° and 120°, respectively. The following equation was used in calculating the adsorption energies:

$$E_{\text{ads,X}} = E_X + E_T - E_{\text{T-X}} \quad (4.1)$$

where E_X , E_T and E_{T-X} are the total energies for the different adsorbates, and for the templates T with and without an adsorbed species X, respectively. This corresponds to the adsorption process:



where T^\bullet is the template modelling the different c-BN (111) cluster surfaces, and X^\bullet is the adsorbed species (H, F, Cl or Br).

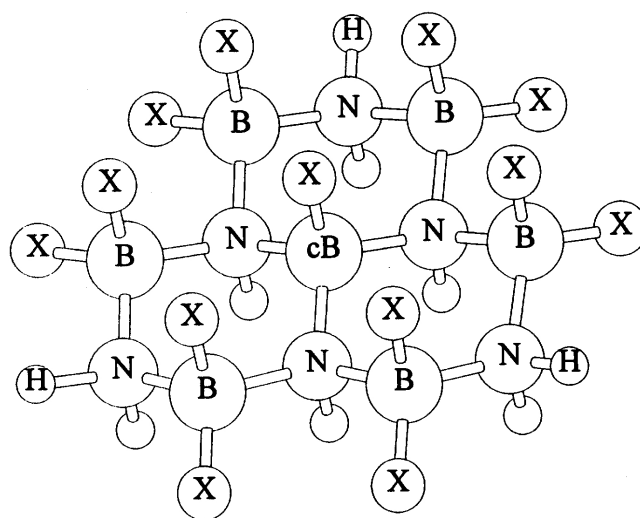


Figure 4.1. An X-terminated BN cluster with (111) geometry ($X = H, F, Cl$ or Br). The same geometry is valid for both B- and N-rich (111) surfaces. However, for the N-rich cluster, B is replaced by N (and vice versa) and cB is replaced by cN as adsorption site.¹

It was found that, with one exception, all terminating species investigated in **paper I** would sufficiently sustain the sp^3 -hybridisation of c-BN (111) clusters. The angles \angle_{NcBN} and \angle_{BcNB} were all ranging between $\approx 109^\circ$ and $\approx 111^\circ$, whereas a partial transformation from sp^3 - to sp^2 -hybridisation was observed for H termination of the N (111) cluster surface ($\angle_{BcNB} = 113.0^\circ$). The interatomic distances indicated that sterical hindrance will be induced by Br species on both types of (111) cluster surfaces, and by Cl species on the N (111) surface. The other terminating species resulted in interatomic distances close to the bulk value.

In Table 1 (page 34), it can be seen that the F species was found to be strongly bonded to both types of c-BN (111) cluster surfaces (273 (B (111)) vs. 223 (N (111)) kJ/mol). The H species, however, showed rather small adsorption energies (106 (B (111)) vs. 130 (N (111)) kJ/mol).

The terminating species must not be too strongly bonded to the surface, and thereby blocking the available surface sites. They must also be able to undergo abstraction reactions with gaseous species and, hence, leave room for an incoming growth species. An abstraction of the central adsorbed species X, thus producing a radical surface site, resulted in a B (111) radical surface that almost totally collapsed at the radical site ($\angle_{\text{NcBN}} \approx 118\text{-}119^\circ$). The neighbouring terminating atoms are thus not able to sustain the sp^3 -hybridisation of the radical boron surface atom. On the corresponding radical N (111) clusters, only a local partial transition to sp^2 -hybridisation was observed ($\angle_{\text{BcNB}} \approx 113^\circ$).

Neighbouring radical sites

As was indicated above, it is of a general interest to study the influence of the surface radical density on structural geometry and adsorption processes. In **paper I**, the influence of neighbouring radicals on structural geometry and hybridisation of the c-BN surface atoms (i.e. reconstruction) was investigated. Based on the results from the investigation on small clusters, where F species was found to be the most efficient surface stabiliser, the surface atoms of the larger clusters were F-terminated. The two larger clusters used were $\text{B}_{10}\text{N}_9\text{H}_{13}\text{F}_{17}$ (representing a B (111) surface), and $\text{B}_9\text{N}_{10}\text{H}_{13}\text{F}_{17}$ (corresponding to an N (111) surface). These templates can be described as five puckered B_3N_3 -rings fused together (instead of three as in Fig. 4.2). They were designed to investigate the influence on structural geometry of two neighbouring radical surface sites. Only the surface atoms and their surface adsorbates were allowed to fully relax during the geometry optimisation. The subsurface atoms and their terminating species were kept fixed in order to resemble a more rigid c-BN cluster. Albeit still being a cluster, it will have less ability to geometrically relax and thus behave somewhat more surface-like.

It was found that the larger (and more rigid) B (111) cluster react very similar to the small, fully optimised one. The larger B (111) cluster surface collapses when the surface terminators are abstracted, however, to a somewhat lesser extent compared to the small cluster ($\angle_{\text{NBN}} \approx 117^\circ$ vs. $\approx 119^\circ$). The boron radical surface sites of both types of clusters are resonance stabilised by hyperconjugation interaction.⁶ This is a resonance interaction in which the radical electron in a p-type orbital on the central radical B (cB) atom interacts with an adjacent B-N bond that is aligned with it. This gives partial double bond character to the cB-N bonds and weakens the aligned B-N bonds. Upon adsorption of F atoms to the collapsed surface sites, the c-BN cluster surface restructures from its collapsed geometry.

The corresponding larger N (111) cluster surface undergoes only a partial transition from sp^3 - to sp^2 -hybridisation when the diradical surface is produced ($\angle_{\text{BcNB}} \approx 113^\circ$), which is identical to the partial hybridisation transition occurring for the small cluster. The N (111) cluster with two unterminated surface sites is then similarly restructured when F species were adsorbed. Hence, it can be concluded that the N-rich

(111) cluster surfaces can withstand a concentration of unterminated surface sites of roughly 20 % without collapsing, whereas the B (111) cluster surfaces will be subjected to a more severe reconstruction. It thus appears that the B-rich of the two different c-BN (111) surfaces (B- or N-rich) is responsible for the difficulties in c-BN growth since it requires to be fully terminated, or else it will collapse.

4.2. Cubic BN (111) Surfaces

General

If small clusters can be stabilised, a crystalline surface with its supportive subsurface layers is most likely also stabilised. The role of atomic hydrogen in diamond CVD growth, both as a preferential etching agent of sp^2 carbon and as a stabiliser of the sp^3 structure, is well known.^{1,2,7,8} In the previous section, it was concluded that both H and F species are effective in stabilising cubic BN (111) clusters. The next step is then to investigate their ability to also stabilise crystalline c-BN (111) surfaces.

In experiments with DC plasma CVD, using a gas-phase mixture with Ar, N_2 , BF_3 and H_2 , it has been found that fluorine is an effective etchant of sp^2 -bonded BN. Furthermore, hydrogen was found to be necessary in producing thin films of BN from the gas phase. However, a too high percentage of hydrogen resulted in h-BN deposition.⁹ In a theoretical investigation regarding the thermodynamic equilibrium, it was observed that both atomic hydrogen and molecular fluorine will react with the solid phase of boron nitride.¹⁰ Thus, both hydrogen and fluorine seem to play an important role in BN CVD.

Adsorption

A six-layer thick slab with periodic-boundary conditions was used in **paper I** in order to study the adsorption of H and F, respectively, to a more realistic crystalline surface of c-BN. A super-cell approach was then used. The six-layer slab was included in a unit-cell with vacuum regions in one direction, while keeping the periodicity in the other two. In addition to the surface terminating H (and F) atoms, three layers of atoms were then allowed to relax.

Significant increases in adsorption energies for the terminating H and F species, respectively, were obtained on this crystalline c-BN (111) surface compared to the small cluster surfaces (Table 1). The numerical values were, with one exception, increased by more than 300 kJ/mol. The F adsorption resulted in similar adsorption energies regardless of model used (cluster or crystalline surface). It can also be seen

that the order of adsorption energy, obtained for the B (111) surface, is similar when using either of the two models (crystalline surface vs. cluster). The F species was then found to be more strongly bonded than H.

On the contrary, a reversed order of adsorption energy was obtained for the N (111) surface. For the crystalline surface, the H species was found (in comparison to F) to be extremely effective as a surface stabilising agent. The F species was slightly more effective on the much smaller cluster surface. Hence, the H species is regarded to be more efficient as an N (111) surface-terminating agent only for more realistic crystalline c-BN surfaces.

In an earlier surface study at the MP2 level of theory, similar adsorption energies (as in **paper I**) were obtained for H and F species adsorbed on the B (111) surface of c-BN (442 vs. 653 kJ/mol).¹¹ The B (111) surface was then modelled as a cluster of identical size as that in Fig. 4.1. In contrast to the calculations in **paper I**, only the atoms closest to the adsorption site were then allowed to relax during the geometry optimisation. The other atoms were kept fixed in order to hold the characteristics of the bulk material underneath the surface plane. Test calculations were also performed using a six-layer slab with periodic boundary conditions (identical to the model used in **paper I**). It was then (in Ref. [11]) concluded that the cluster model will sufficiently describe the c-BN (111) crystalline surface.

Based on these results it is possible to draw the conclusion that this type of constraints is compulsory when modelling a crystalline surface. It is thus not motivated to use a computationally more demanding slab model, when studying energetics and geometrical structures of c-BN (111) surfaces.

<i>Adsorption energy</i>	B (111)		N (111)	
	<i>Cluster</i>	<i>Surface</i>	<i>Cluster</i>	<i>Surface</i>
H	106	482	130	438
F	273	690	223	251

Table 1. Adsorption energies (in kJ/mol) of H and F species on c-BN (111) clusters and crystalline surfaces.

Abstraction and migration of terminating species

Different types of terminating species (e.g., H, F) must be sufficiently strongly bonded to the BN surface in order to stabilise the desired cubic phase. However, they must not be too strongly bonded to the surface, and thereby blocking the available surface sites. An abstraction of the terminating species with gas phase species, or a high enough surface mobility, is needed for a continuous growth of the c-BN phase. Hence, gas phase abstraction, as well as migrational jumps between neighbouring surface sites, were also investigated in **paper I** using the more realistic crystalline surface mentioned above (clusters with constrained geometry optimisation). Both the H- and F-terminated c-BN (111) surfaces were then assumed to undergo abstraction reactions with gaseous H and F species, respectively. It was found that the abstraction process of adsorbed H species (with H (g)) and adsorbed F species (with F (g)) on the N (111) surface, were markedly weakly endothermic (45 vs. 28 kJ/mol). The corresponding abstraction of adsorbed H species on B (111) was found to be somewhat stronger endothermic (123 kJ/mol). The situation, however, was found to become more severe for adsorbed F species on the B (111) surface. They will most probably block the surface, and thereby hinder any further c-BN growth (an abstraction energy of 542 kJ/mol).

The migration process investigated in **paper I** was assumed to involve two neighbouring surface radical sites. Migration of H and F, respectively, was then assumed to occur as a single jump between two radical surface sites. A transition state (TS) was located on the potential energy surface, and the energy barrier was calculated as the difference in energy between the TS and the adsorbed configuration. The calculated energy barriers for the assumed migration path, resulted in a conclusion similar to the one obtained from the abstraction study; The F species will block the B (111) surface for further growth, whereas the surface stabilising H atoms is more mobile. On the N (111) surface, a relatively small energy barrier for the assumed single jump migration path was calculated for F species. The migration barrier of H was, however, found to be higher. All together, the main conclusion is that H is (compared to F) very efficient as a terminating species since it has a larger probability for *i*) being bonded to and, hence, stabilise both the B (111) and the N (111) surface, and *ii*) leaving room for an incoming growth species to the c-BN (111) surfaces (both B- and N-rich).

4.3. Nucleation on h-BN

Introduction

It is of vital importance to suppress formation of “non-cubic” BN in order to have a controlled c-BN growth. This can be achieved, either by etching or by a preferential nucleation of the cubic phase of BN on the hexagonal one.

As described in *Chapter 1*, it has been observed experimentally that hexagonal BN either functions as a “substrate” for c-BN growth (in PVD methods) or as the actual resulting film (in TACVD and HF-CVD). In diamond CVD, hot-filament experiments have demonstrated the usefulness of h-BN as substrate for diamond growth without specifying whether the nucleation occurs on the basal plane or on the edges of h-BN (001).¹² Furthermore, several experimental studies report on a transformation from sp^2 to sp^3 for a-BN and h-BN surfaces when they are treated in a plasma with hydrogen.¹³⁻¹⁵

The structure of PVD films of boron nitride most often follow the widely accepted model of a layered growth in the sequence; a-BN/h-BN/c-BN (see Fig. 1.2).¹⁶⁻¹⁸ Based on results from a RF-sputtering process (PVD), it has been observed that the cubic BN crystallites nucleate on the edges of the h-BN planes in such a way that the c-BN initially nucleates in an ordered [111] growth direction on the edges of the (002) planes of h-BN.¹⁹ A high compressive stress, induced by ion bombardment, in the well-oriented layer of h-BN is thought to be necessary for the nucleation of the cubic phase.²⁰ The induced stress would then provide sufficient energy for a phase transformation. The question is whether a heterogeneous nucleation of c-BN on h-BN is thermodynamically possible during e.g. a CVD process? Is it for example possible to nucleate cubic BN without using stress? A series of studies have, hence, been conducted in order to achieve a deeper understanding of the nucleation process of c-BN on h-BN. In the first study, the nucleation on the basal plane was investigated (**paper II**), whereas the other two studies were devoted to nucleation on the basal plane edges of h-BN (**papers III and IV**).

Transformation from sp^2 to sp^3 on the basal plane

Conditions of supersaturation of either H or F in the gas-phase were assumed in **paper II**. These conditions are met in e.g., a hot-filament or plasma CVD reactor. The H or F species were then thought to adsorb on either B or N surface atoms in the h-BN basal plane. If the surface atoms are adapting the sp^3 -hybridisation configuration, the adsorbing surface atom (and its adsorbed species) can be regarded as an embryo of a c-BN nucleus. This “embryonic” nucleus may thereafter undergo further reactions with the gaseous phase, resulting in the formation of a larger c-BN nucleus.

Three differently sized clusters were used in modelling the h-BN (001) surface in **paper II** (Fig. 4.2). The smallest ($B_7N_7H_{10}X$), medium-sized ($B_{10}N_{10}H_{14}X_2$) and largest ($B_{12}N_{12}H_{17}X_3$) clusters contain one, two and three adsorption sites, respectively ($X = H$ or F). The medium-sized and largest clusters were predominantly used in order to investigate a substitutional effect further away from the observed adsorption site (see below).

The geometrical and energetic parameters investigated in **paper II** are *i*) the substrate-adsorbate distances, *ii*) the angles \angle_{NBN} and \angle_{BNB} of the adsorption sites B and N, respectively, and *iii*) adsorption energies for the two adsorbates (H and F) on both B and N sites.

For an ideal h-BN (001) surface, it was geometrically observed that the adsorption of F on the surface B atoms, and the adsorption of H on the surface N atoms, would lead to the formation of small embryonic c-BN nuclei. The surface angles \angle_{NBN} and \angle_{BNB} (both $\sim 111^\circ$) indicate that the adsorbing surface atoms have been locally transformed from sp^2 -hybridisation to an almost complete sp^3 -hybridisation state. The accompanying adsorption energies were 313 (B-F) and -55 (N-H) kJ/mol, respectively, indicating that only the fluorine species will be able to provoke the formation of an embryonic c-BN nucleus.

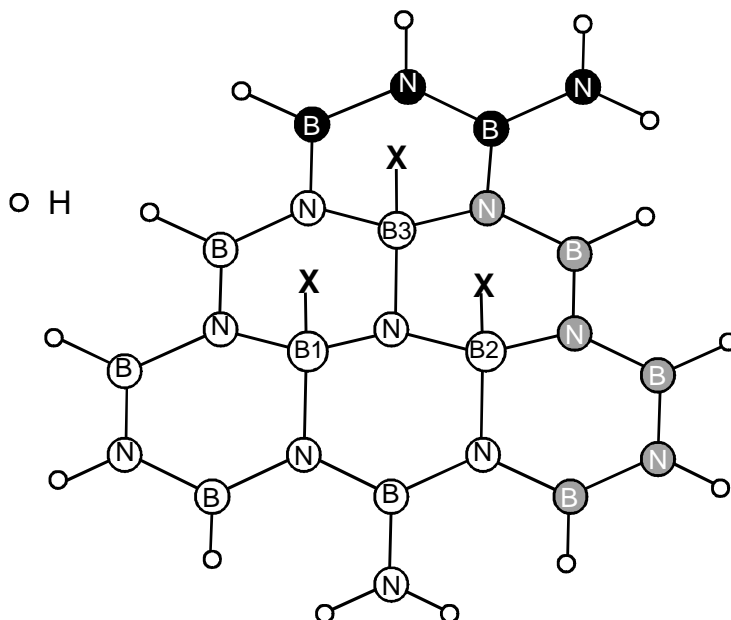


Figure 4.2. A model representing the h-BN (001) cluster. The geometry is also valid for the h-BN (001)-N surfaces. The B atoms are then replaced by N atoms, and vice versa. The white atoms represent a cluster with one adsorption site (B1). A second (B2) and third (B3) adsorption site will be included by adding the greyish and black atoms.

Boron, nitrogen and carbon can form ternary compounds like BC_2N or BC_4N ,²¹ as well as composite $\text{B}_x\text{C}_y\text{N}_z$ nanotubes and nanofibres.^{22,23} Furthermore, BN can be both p- and n-doped with e.g., carbon.⁵ By substituting B atoms with C atoms in different positions in the h-BN (001) surface plane, electrons were introduced into the system and interesting effects were observed. Firstly, not only F species but also H species were chemisorbed on a B site, thereby resulting in a transformation from sp^2 - to sp^3 -hybridisation for the adsorbing surface B atom. Secondly, the adsorption energies of both H and F species atoms on a B site increased by 130 – 140 kJ/mol.

It thus appears as if the extra electron is concentrated to the B-H/F bond, and subsequently strengthens it. However, the electron absorption effect was local. The further away the substituted C atom was located from the adsorbing B atom, the less sp^3 character it adapted. This local effect was also observed in an LMTO-ASA-ES calculation of the electronic structure of c-BN by Zhang et al.²⁴ They stated that impurity carbon atoms would predominantly affect the density of states of its nearest neighbouring atoms.

An electron deficient surface was produced, by substituting an N atom with a C atom. Both the structural geometry and the adsorption energy for a B site was then negatively affected (i.e., a more pronounced sp^2 character of the adsorbing surface atom was observed, and the adsorption energy decreased). In contrast, the electron deficiency positively affected the hydrogen adsorption for an N site; e.g., the N-H bond was strengthened by 110 kJ/mol.

Conclusively, the B atoms in the basal plane of h-BN (001) will most probably have the capability to form embryonic c-BN nuclei (provided the gaseous environment is electron-rich as in plasma or hot-filament CVD). Furthermore, the sp^3 character of these surface B atoms is decreasing when going from an electron-rich to an electron-deficient surface. On the other hand, the N atoms of the h-BN basal plane were found to less likely participate in any formation of embryonic c-BN nuclei. This contradicts the experimental observations from PECVD with hydrogen. It was there observed that the H atoms preferentially adsorb on N sites of sp^2 -hybridised BN, and thus transform them to sp^3 -hybridisation.²⁵

Nucleation on the h-BN (001) edge atoms

In Fig. 4.3 a), the interface between the layers of well-oriented hexagonal BN and cubic nanocrystalline BN can be seen. Fig. 4.3 b) illustrates a small H-terminated cubic BN nucleus just as it has been formed on the h-BN basal plane edge atoms.

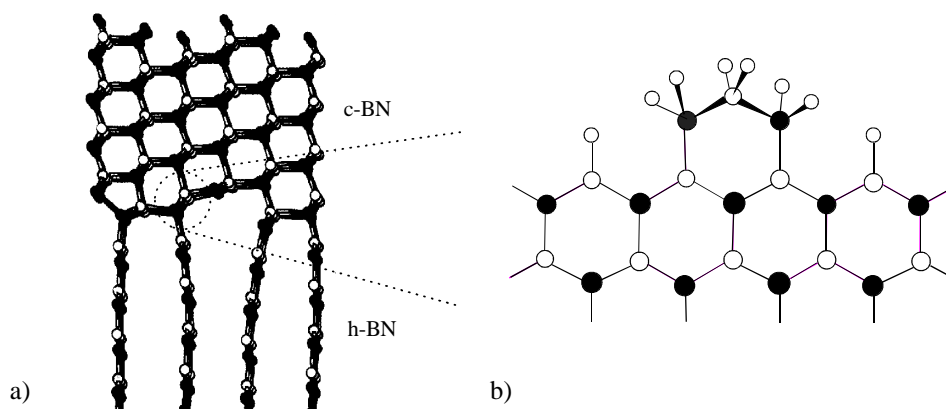


Figure 4.3. A model of a) the interface between the oriented (c -axis \parallel substrate) hexagonal BN layer and the cubic BN layer (from Ref. [26]), and b) an H-terminated cubic nucleus on the h-BN (001) zigzag edge.

The edge atoms are allowed to be H-terminated by adsorption of atomic hydrogen from the gaseous phase. This has earlier been shown to be energetically favourable for graphite sheets.²⁷

The h-BN basal plane exhibits three different edges. The three edges include two zigzag edges (boron atoms on the (100) edge and nitrogen atoms on the $(\bar{1}00)$ edge) and the armchair edge (a combination of boron and nitrogen atoms on the (110) edge) (see Fig. 4.4).

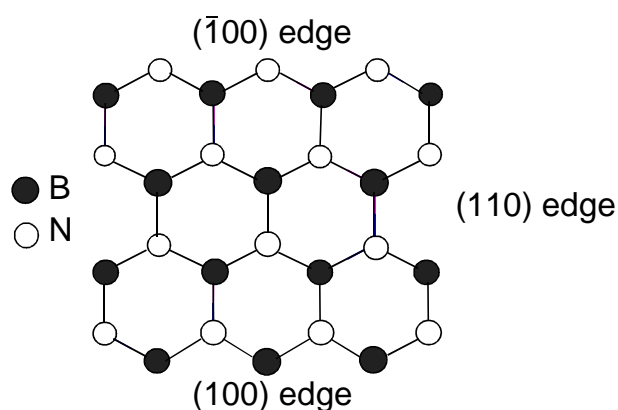


Figure 4.4. A model of a non-terminated h-BN (001) basal plane, demonstrating the $(\bar{1}00)$, (100) and (110) edge, respectively.

The mechanism of the c-BN nucleation is assumed to involve adsorption of B- or N-containing species (e.g., BF_3 , NH_3), as well as abstraction of terminating H or F species. The individual steps are then also assumed to result in the completion of a six-membered ring (buckled or planar) of alternating boron and nitrogen atoms. The details in the various mechanisms were not explicitly studied in **papers III** and **IV**. What was of most interest was instead the difference in total energy for the corresponding buckled and planar outgrowths, i.e., the thermodynamic stability favouring either the cubic or hexagonal nuclei.

To calculate the stabilisation of the buckled (c-BN or w-BN) outgrowth in relation to the planar (h-BN) counterpart, the following formula was used;

$$\Delta E = E_{\text{planar}} - E_{\text{buckled}} + nE_X \quad (4.3)$$

where E_{planar} and E_{buckled} are the calculated total energies for the planar and buckled outgrowth, respectively, and E_X is the total energy for an H or F atom (depending on the type of termination of the outgrowth). The relative energies have to be balanced by the difference in number of terminating species (n) for the planar and buckled outgrowths (see Fig. 4.5).

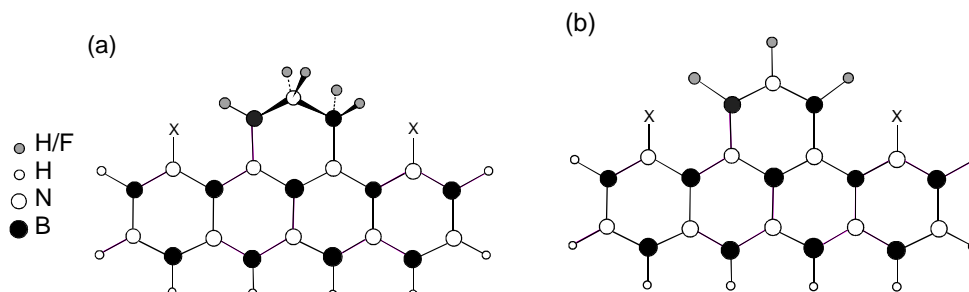


Figure 4.5. An illustration of (a) *c*-BN and (b) *h*-BN nucleation on a template modelling the $(\bar{1}00)$ edge of the *h*-BN (001) plane. The greyish atoms are either terminating H or F species. The terminating species “X” (neighbouring the outgrowth) are either H or F.

In **paper III**, the different outgrowths, cubic or hexagonal, are derived from arbitrary growth species. As a continuation of **paper III**, nucleation of *c*-BN from experimental growth species formed between Lewis acid-base pairs such as BX_3 ($\text{X} = \text{F}, \text{Cl}$ or H) and NH_3 , was studied in **paper IV**. The adducts ($\text{X}_3\text{B}:\text{NH}_3$) have experimentally been observed in TACVD with BCl_3 and NH_3 as precursors or in PECVD with a mixture of B_2H_6 , NH_3 and H_2 as precursors.^{28,29} Furthermore, the chemical reactions between BX_3 ($\text{X} = \text{F}, \text{Cl}$ or H) and NH_3 are important in BN chemistry and have been subjected to many investigations.³⁰⁻³³ The resulting adduct $\text{X}_3\text{B}:\text{NH}_3$ is an unstable solid at room temperature and will readily eliminate HX to form X_2BNH_2 .³⁴⁻³⁶ The gas-phase reactions in a TACVD reactor between BCl_3 and NH_3 have been experimentally and theoretically investigated.^{28,37,38} Cl_2BNH_2 was identified as the major boron-containing compound, with $\text{ClB}(\text{NH}_2)_2$ being less abundant but still present.²⁸ In the borane-ammonia PECVD reactor, the metastable species BNH_x ($\text{X} = 1-4$) are thought to play an important role in *c*-BN gas-phase synthesis.^{39,40} In addition, because of the high electronegativity of F and the common use of BF_3 in BN CVD, fluorine-containing precursors were also considered in **paper IV**. The reactions between BF_3 and NH_3 were then thought to be consistent with the reactions between BCl_3 and NH_3 .

For example, on the B rich (100) edge, a nucleus can be constructed from two adsorbed X_2BNH_2 complexes resulting in a nucleus consisting of an NBN skeleton (H and X are omitted for simplicity) and a BX_2 tail (Fig. 4.6 (a)). The nucleus can also be constructed from $\text{XB}(\text{NH}_2)_2$, resulting in an NBN skeleton without a BX_2 tail (Fig. 4.6 (b)). The outgrowths derived from the gaseous precursors X_2BNH_2 and $\text{XB}(\text{NH}_2)_2$, will thus differ in the numbers of B and N atoms. In an earlier study, *c*-BN clusters were found effectively stabilised when built up from equal numbers of B and N atoms.⁴¹ Therefore, in the case of nucleation from $\text{XB}(\text{NH}_2)_2$, an extra BH_2 group will be added to the *h*-BN (001) template.

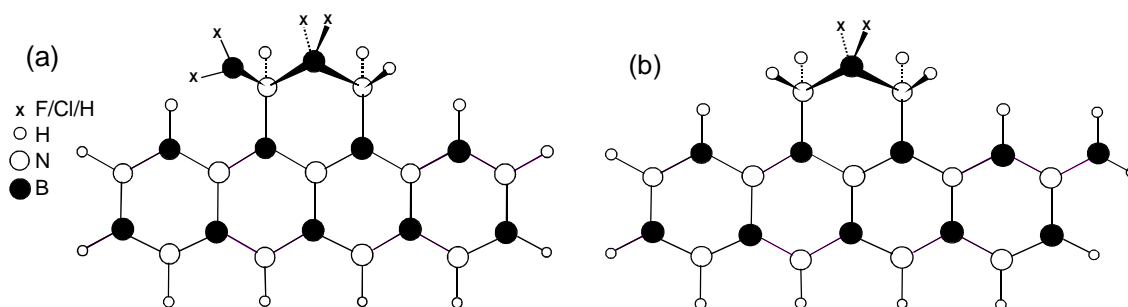


Figure 4.6. An illustration of *c*-BN nucleation on a template modelling the (100) edge of *h*-BN (001). The outgrowths are derived from (a) two gaseous X_2BNH_2 and (b) one gaseous $XB(NH_2)_2$ species.

In an earlier investigation concerning diamond nucleation on terminated *h*-BN (001) zigzag edges, it was concluded that neither electronegative (F or OH), electropositive (Na) nor bulky (CH_3) neighbouring terminating species had a large effect on the difference in energy between a buckled and a planar outgrowth.^{42,43} In contrast to diamond, boron nitride is a polar compound. The question is then: How is the nucleation of *c*-BN affected by different neighbouring terminating species (with varying electronegativities)? The possible influence of edge termination was studied in **paper III** by applying a termination on the edges, different from that on the outgrowths (Fig. 4.5). It could then be concluded that neighbouring, terminating species (H or F) have little effect on the stability of cubic nuclei of BN.

The calculations show that in an H- or F-rich environment, the nucleation of *c*-BN along the zigzag edges, as well as along the armchair edge of *h*-BN (001), is energetically more favourable than a corresponding nucleation of *h*-BN. On the armchair edge, the nucleation of *w*-BN is even more energetically preferred than the nucleation of *c*-BN, albeit the differences between the two sp^3 -bonded phases are small. The calculations presented in **paper III** clearly show that the nucleation of *c*-BN is energetically favoured over a continuous growth of *h*-BN (Fig. 4.7). The species H or F, terminating the edge-atoms closest to the different outgrowths, were shown to have only a minor effect on the relative nucleation stability.

The F-terminated cubic outgrowths show the highest numerical value of relative energy for all three edges investigated, regardless of whether the outgrowths are derived from arbitrary or experimental growth species. For the Cl- and H-terminated ones, it was found that the order of relative energies on the different edges was not consistent, but changed (Fig. 4.8). However, the energy differences between the two types of terminations were not very large (~50-115 kJ/mol). This similarity in energy stabilisation can to some extent explain the interchange in the order of stability for the Cl- and H-terminated outgrowths.

As can be seen in Fig. 4.7, the F-terminated outgrowths derived from arbitrary growth species (**paper III**) are more stable than the corresponding H-terminated ones for all edges investigated. The difference in stability (in relation to H-terminated outgrowths) are ~ 160 , ~ 180 and ~ 190 kJ/mol for the edges (100), $\bar{(100)}$ and (110), respectively. Moreover, the following order of cubic stability was observed for the various edges (for both H- and F-termination); $(110) \gg \bar{(100)} \approx (100)$.

For outgrowths derived from experimental growth species (**paper IV**), the following order of cubic stability is observed for all types of termination; $(110) > \bar{(100)} > (100)$ (Fig. 4.8). The (110) and $\bar{(100)}$ edges show almost identical ability in stabilising the cubic nuclei when using F-terminated outgrowths. This is also the situation for the $\bar{(100)}$ and (100) edges when using H-terminated outgrowths.

It can be seen that the differences in relative energy between outgrowths derived from the two types of experimentally found gaseous species (X_2BNH_2 and $XB(NH_2)_2$) are less than 120 kJ/mol for all cases investigated (**paper IV**). From a thermodynamic point of view, none of the two types of gaseous complexes can therefore be said to be a preferred precursor. However, the Cl_2BNH_2 group is found to be the most abundant one in the gas-phase ($\sim 10:1$), which indicates a preference for an Cl_2BNH_2 adsorption.²⁸

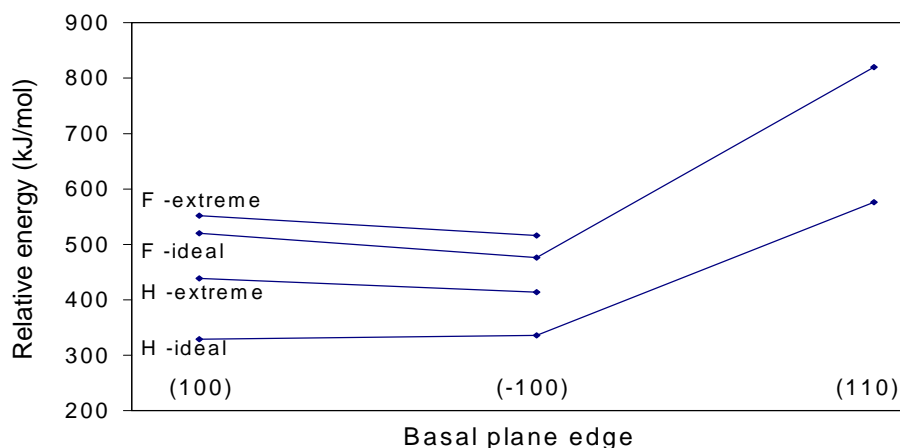


Figure 4.7. Relative energies obtained for the nucleation of cubic BN on the (100), $\bar{(100)}$ and (110) edge atoms of the h-BN basal plane. Nucleation in an ideal, and in an extreme environment for H- and F-terminated outgrowths.

As a test of the behaviour of BN growth in an extremely reactive and radical rich environment, the hypothesis of extra adsorption of H or F to the various outgrowths was investigated. On the $\bar{(100)}$ edge, it leads to the production of an ionic $[B(X_2)-N(X_2)-B(X_2)]^-$ and $[B(X)-N(X)-B(X_2)]^-$ type of outgrowth for the buckled and planar

outgrowths, respectively. The relative energy for the ionic case is then compared to the relative energy for the more likely *neutral* situation. On the (100) edge, the adsorption of an extra species leads to the formation of a *radical* $[N(X_2)-B(X_2)-N(X_2)]$ or $[N(X)-B(X)-N(X_2)]$ type of outgrowth. The relative energy for these radical outgrowths is compared to the *non-radical* situation. If the adsorption do occur, it is thought to be of an extremely short-lived character. The neutral and the non-radical situations and outgrowths are jointly labelled *ideal*.

It is observed that the order of cubic stability for both H- and F-termination in an extreme environment, is similar to the ideal situation; $(100) \approx (\bar{1}00)$ (Fig. 4.7). Furthermore, there is an almost identical probability to obtain either a neutral or a radical/ionic F-terminated outgrowth in CVD growth of c-BN. However, the ideal H-terminated outgrowths show a weak tendency for adsorbing an extra radical H species and, hence, become radical or ionic outgrowths, respectively. These results strongly support a thermodynamically favoured c-BN nucleation on h-BN.

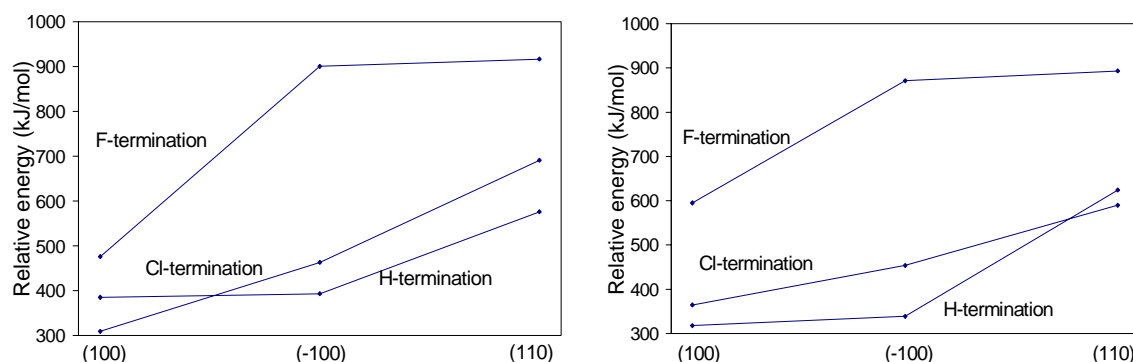


Figure 4.8. Relative energies obtained for the nucleation of cubic BN on the (100), $(\bar{1}00)$ and (110) edge of the h-BN basal plane. The outgrowths were derived from (left) X_2BNH_2 , and (right) $XB(NH_2)_2$.

When summarising the nucleation investigations in **papers III** and **IV**, it can clearly be seen that regardless of whether the cubic BN nuclei are derived from arbitrary or experimental (TACVD or PECVD) growth species, they are significantly more stable than their hexagonal counterparts. This is especially the situation with F-terminated nuclei. Furthermore, the cubic BN nuclei have an equal probability to be formed either in an ideal or in an extremely radical-rich environment. It should, however, be stressed that **papers III** and **IV** only address the relative tendency, and not the total ability for BN nucleation on h-BN (001) edges.

4.4. Boron deposition

Introduction

Thin films of boron nitride and elemental boron, both part of the B-N system, exhibit somewhat similar properties. They are light, refractory materials with high hardness, high mechanical strength and low chemical reactivity at room temperature.^{5,44} However, whereas boron nitride is an insulator (bandgap of > 5 eV),⁴⁵ boron exhibits semiconducting behaviour (bandgap = 1.5 eV)⁴⁶ and it is a good thermal neutron absorber.⁴⁴ Because of the attractive properties of boron, it has found significant applications in the production of protective and refractory coatings, fibre-reinforced composites, and electronic components, as well as in the area of nuclear protection in fission reactors.

Boron thin films can be deposited by chemical vapour deposition (CVD) from a boron halide (BCl_3 or BBr_3). The boron halide is then reduced with hydrogen in a reactor.^{47,48} The mechanism and kinetics of boron deposition has been experimentally studied whereby several species have been identified in the gas phase; H_2 , HX , X_2 , BHX_2 and BX_3 ($\text{X} = \text{Cl}$ or Br).⁴⁷⁻⁴⁹

Despite the technological interest in boron thin films, only few theoretical studies have been performed. These investigations report on the adsorption of monatomic hydrogen onto $\text{B}_{12}\text{H}_{12}$ clusters, and the adsorption of molecular hydrogen on boron cluster surfaces.^{50,51} The $\text{B}_{12}\text{H}_{12}$ cluster study (on the MP4 level of theory) concluded that the adsorption of monatomic hydrogen is only energetically favourable when centred on a B-B edge.⁵⁰ In the investigation concerning boron cluster surfaces (on the HF level of theory) it was found that upon adsorption H_2 may in some cases dissociate, resulting in the bonding of hydrogen atoms to different boron atoms on the cluster surface.⁵¹ This will be the situation when a) H_2 is approaching an open pentagonal surface (*nido*- B_6) and when b) H_2 is approaching the α -B surface “between” two boron icosahedra.

In **paper V**, the interaction of gaseous H_2 , Br_2 and HBr with an α -boron (001) surface was investigated. The cluster model chosen was the boron icosahedron, B_{12} . As was experimentally determined by Decker and Kasper, the B_{12} -units are arranged according to the rhombohedral α -B structure.⁵² Direct B-B bonds in α -boron will bind adjacent B_{12} -units to each other (Fig. 4.9). The bonding distance is 2.03 Å. As can be seen in Fig. 4.9, the bonding situation within the B_{12} icosahedron can be described as two unequal sets of six atoms each. The two sets consist of polar (3 + 3) atoms and six equatorial atoms, respectively. The polar sets can be observed as two triangles in Fig. 4.9. One facing upwards (situated just above the paper plane) and the other facing downwards (just below the plane). The equatorial set of six B atoms forms a hexagon along the equator of the icosahedron, midway between the two triangles.

The B-B distance is 1.733 Å (within the polar set) and 1.777 Å (within the equatorial set), respectively. The bonding distance between the sets is 1.787 Å. However, both amorphous and α -boron may be formed during deposition of boron thin films (the phases differ only in the long-range order).⁵³ The boron surface may thus display different B-B edges to the incoming gaseous species. For the different edges, calculated adsorption energies and migration barriers are, however, unlikely to differ significantly due to small differences in B-B bond length (0.01 – 0.05 Å).⁵⁰ An “average surface” with equivalent B-B distances of 1.77 Å was therefore chosen as a most realistic model in **paper V**.

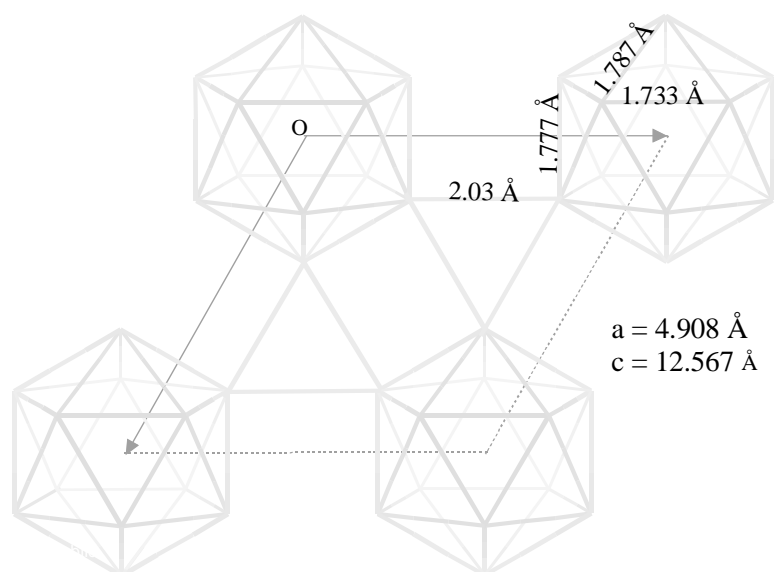


Figure 4.9. The (001) surface of α -B,⁵² with boron icosahedra at the corners of the unit cell. Two sets of three B atoms are facing up- and downward in each B_{12} -unit, forming “polar” triangles. The remaining six B atoms, forming a “hexagonal” frame viewed from this angle, are then in the equatorial position. Interatomic distances are given for each type of bond.

Adsorption

To test whether the adsorption of the diatomic molecules H_2 , Br_2 and HBr occurs dissociatively or not, a potential energy surface (PES) was created by manually and stepwise decreasing the distance between the molecule and the boron surface. Then starting at a distance of 8.00 Å with a following decrease in distance of 0.50 Å. When there was an increase in total energy, the increment was allowed to decrease. Simultaneously, the accompanying distance between the atoms of the incoming molecular species had to be stepwise increased from the bonding, gas-phase value to the corresponding non-bonding value (at equilibrium surface-adsorbate distance).

The PES of H_2 and Br_2 approaching the boron surface is demonstrated in Fig. 4.10. For hydrogen, the obtained energy minima represents a dissociative chemisorbed state with a bonding B-H distance of 1.21 Å. The adsorption energy was calculated using

equation (4.1) (page 24), and for the hydrogen atoms it was found to be 290 kJ/mol. The energy barrier for dissociative adsorption of H_2 was 190 kJ/mol. For bromine, the B-Br distance for the dissociative chemisorbed state was 2.01 Å. The adsorption energy for the bromine atoms was 397 kJ/mol. The energy barrier for dissociation of the bromine molecule is only 24 kJ/mol. A tendency for a weak, physisorbed state can be observed in the PES diagram for Br_2 . For the physisorbed state, the B-Br distance is 4.62 Å (Br-Br (bonding) = 2.33 Å). The corresponding ΔE_{phys} for Br_2 is 11 kJ/mol.

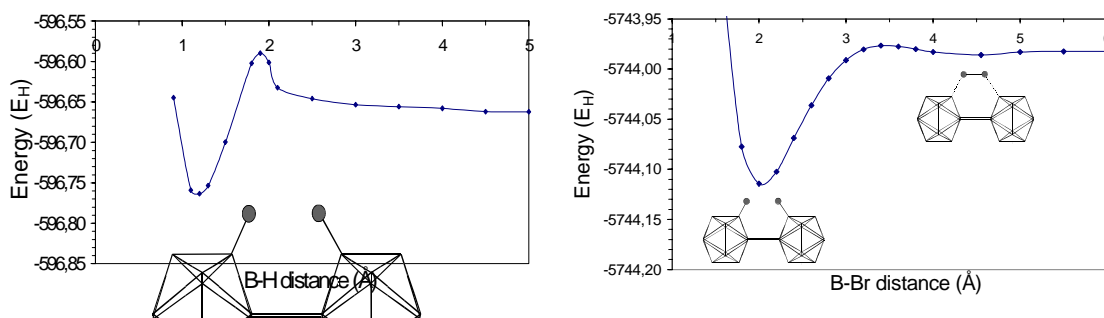


Figure 4.10. A potential energy surface for the approaching (left) H_2 molecule, and (right) Br_2 molecule towards the boron surface (in between two B_{12} icosahedra).

From the dissociative adsorption energies and the corresponding energy barriers, it can be concluded that gaseous Br_2 most likely will become dissociatively adsorbed on the α -boron surface at experimental conditions. The adsorption energy is 397 kJ/mol and the barrier for adsorption is as low as 24 kJ/mol. The adsorption barrier for gaseous HBr is 78 kJ/mol, which also might be overcome at boron deposition temperatures ($>900K$).⁵⁴ However, the high energy barrier for dissociative chemisorption of H_2 (190 kJ/mol) indicates that hydrogen molecules most likely will not dissociate at the boron surface.

The α -B (001) surface displays three different adsorption sites as shown in Fig. 4.11. The different sites are labelled a) atop, b) bridge and c) hollow site. The atop site has already been investigated above. This site was also, as a result of ordinary geometry optimisation calculations, found to be the thermodynamically most stable one. Hence, if the adsorbates were allowed to be totally relaxed, in the bridge or hollow position, the resulting geometry were in all cases the atop position. Therefore, to be able to estimate an adsorption energy for the bridge and hollow sites, respectively, the adatom (H or Br) was stepwise allowed to approach the boron surface. The total energies calculated for each step were then recorded until a minimum in total energy was obtained.

The order of adsorption energy for the three most possible surface sites were for both H and Br: atop $>$ bridge $>$ hollow. As been described earlier, the adsorption energy on atop site was greater for Br than for H (by 107 kJ/mol). Furthermore, the Br atom was found to adsorb more strongly (compared to H) also on bridge ($\Delta E_{\text{ads}} = 80$ kJ/mol) and hollow ($\Delta E_{\text{ads}} = 127$ kJ/mol) sites. This is possibly due to a larger orbital overlap between the highly directional bonds of the B_{12} unit and the larger Br atom.

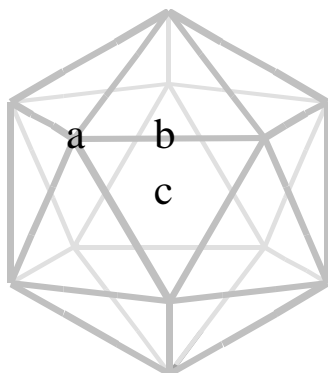


Figure 4.11. A schematic model of a B_{12} icosahedron, displaying three distinct adsorption sites; a) atop, b) bridge and c) hollow site.

Migration and abstraction of adsorbed species

Desorption, through a Langmuir-Hinshelwood mechanism,⁵⁵ of gaseous hydrogen halide has been proposed as the rate-determining step in boron deposition.^{48,56} The production of HX (X = Cl or Br) can be obtained by, a) a surface reaction between two adsorbed species H and X, or b) a reaction between an adsorbed species (H/X) and a gaseous one (H/X). For the reaction between two adsorbed species to occur, they must migrate to adjacent surface sites. For the B_{12} unit the thermodynamically most stable adsorption site for both hydrogen and bromine was the atop site. In **paper V**, the migration between atop sites was therefore studied.

A transition state (TS) for migration between two atop sites was localised on the potential surface in the region between these surface sites. The difference in energy between this TS and the chemisorption situations (to one of the atop sites) was then taken as the barrier of migration.

The resulting migration barrier for H was found to be 191 kJ/mol, which is 99 kJ/mol lower than the adsorption energy for an atop site (290 kJ/mol). The obtained barrier for Br migration is 127 kJ/mol. This is 240 kJ/mol lower than the adsorption energy for Br on an atop site (397 kJ/mol). From the present calculations it is, hence, possible to draw the conclusion that Br species, migrating between the most thermodynamically preferred adsorption sites (atop), has a somewhat higher mobility compared to H.

The reaction energies for the abstraction of *H and *Br was also studied in **paper V**, following either a Langmuir-Hinshelwood (L-H) or an Eley-Rideal mechanism (E-R).^{55,57} The L-H mechanism, involving the reaction between two adsorbed species, was modelled according to the following formula;



$B_{12}^*X^*Y$ can be described as a B_{12} icosahedron with two adsorbed species, each on adjacent sites. The adsorbed species are then presumed to react and desorb as a gaseous, molecular species XY ($X/Y = H$ or Br). The E-R mechanism describes the situation with one adsorbed species, reacting with a gaseous species according to reaction [4]. The energies for this type of abstraction process:



where T is modelling the α -B (001) surface, and X and Y are H or Br, were calculated employing the following formula:

$$E_{\text{abstr, X}} = E_T + E_{X-Y} - E_{T-X} - E_Y \quad (4.6)$$

E_{T-X} , E_Y , E_T and E_{X-Y} are the total energies for the gaseous species X and $X-Y$, respectively and for the template T , with and without an adsorbed species X .

It was found in **paper V** that for the E-R and L-H reactions (producing H_2 , Br_2 or HBr), only two reactions were exothermic: The abstraction of adsorbed hydrogen (or bromine) with gaseous hydrogen (producing $H_2(g)$ and $HBr(g)$, respectively). The resulting abstraction energies were -41 vs. -35 kJ/mol. It should also be noted that the abstraction of adsorbed hydrogen with gaseous bromine (to give $HBr(g)$) was only slightly endothermic (46 kJ/mol). The remaining E-R reaction (abstracting adsorbed Br with gaseous Br) together with all three L-H reactions ($*H-*H$, $*H-*Br$ and $*Br-*Br$) were all found to be highly endothermic (>200 kJ/mol). These results then thermodynamically contradict the experimental observations in Ref. [48]. They investigated by mass spectrometry the reaction kinetics of the gaseous H_2-BBr_3 system in a CVD reactor. In Ref. [48], two plausible L-H reaction mechanisms, differing in the BBr_3 decomposition, were proposed. The first involves the decomposition of $*BBr_3$, which produces $*Br$ that reacts with $*H$ to form $HBr(g)$. The second mechanism, involves the direct abstraction of Br atoms from $*BBr_x$ species by H adatoms to generate $HBr(g)$. None of the mechanisms was found to fit the data at all conditions, but a mechanism involving the abstraction of Br from $*BBr_x$ by $*H$ was most consistent with the experimental results. The fact that no E-R type mechanism was modelled in Ref. [48], and that the proposed L-H mechanism was not unambiguous, may explain the discrepancies between their and our conclusion.

5. ALD OF BORON NITRIDE

5.1. Introduction

In chapter 1, thin film deposition of boron nitride was shortly reviewed, and the problems connected to either the PVD or CVD methods were elucidated. It appears as if it is only a deposition method using less brute force than PVD methods that can surmount the problems of residual stress in PVD films, as well as the problems with the layered structure. The CVD method represents a gentler deposition method and the conditions during a CVD process are often close to equilibrium. Films containing less defects may therefore be deposited.

In CVD methods, the precursors can either be fed into the reacting zone in a continuous flow, or in a sequential flow (by an alternating flow of the different precursors). In a study of surface processes in c-BN growth, it was concluded that a mixture of B- and N-containing species in the gas phase most likely would result in a mixture of B- and N-containing species on the B (111) surface.¹ Furthermore, in that study and in **paper I** it was concluded that fluorine containing species should be avoided since they will most likely produce surfaces that are resistant to abstraction and to further growth of c-BN. Thus, a gas phase chemistry consisting of mobile and less strongly surface-binding stabilisers (e.g., H), and a sequential pulsing of precursors, ought to be optimal in c-BN deposition.

5.2. Atomic Layer Deposition (ALD)

Atomic layer deposition (ALD), originally proposed in 1977 by Suntola and Antson² is a deposition method based on alternating supply of reactants into the reactor. The reactants will thus, separated in time, be subjected to chemisorption, surface reactions and desorption. ALD growth is characterised by its self-limiting deposition process, in which the growth rate is independent of growth parameters such as vapour pressure of the precursors and growth temperature (within the ALD window), but dependent on the number of growth cycles. In ALD, the reaction gases are alternately pulsed into the reactor, which is purged with an inert gas between the reactant pulses. Ideally one monolayer of each reactant is chemisorbed onto the substrate for each pulse. Thus, after one completed cycle, one monolayer of the desired compound has been formed (Fig. 5.1). However, due to sterical hindrances of the chemisorbed precursors, the growth rate is often lower than one monolayer per cycle.³

The deposition of a complete monolayer per cycle is, however, not an absolute requirement. As long as the precursor molecules during each adsorption step occupy the same numbers of adsorption sites, an accurate control of the film thickness is achieved.

The ALD method has several features making it advantageous over conventional CVD methods;⁴ *i*) the self-limiting growth process, which provides a simple thickness control, a good reproducibility, and the capability to produce sharp interfaces and superlattices, *ii*) the alternate supply of precursors which favours precursors highly reactive towards each other, thus enabling efficient precursor utilisation and a lowering of the deposition temperature, and *iii*) a wide processing temperature window, which makes it possible to make multilayer structures in a continuous process. The major drawback is the low growth rate.

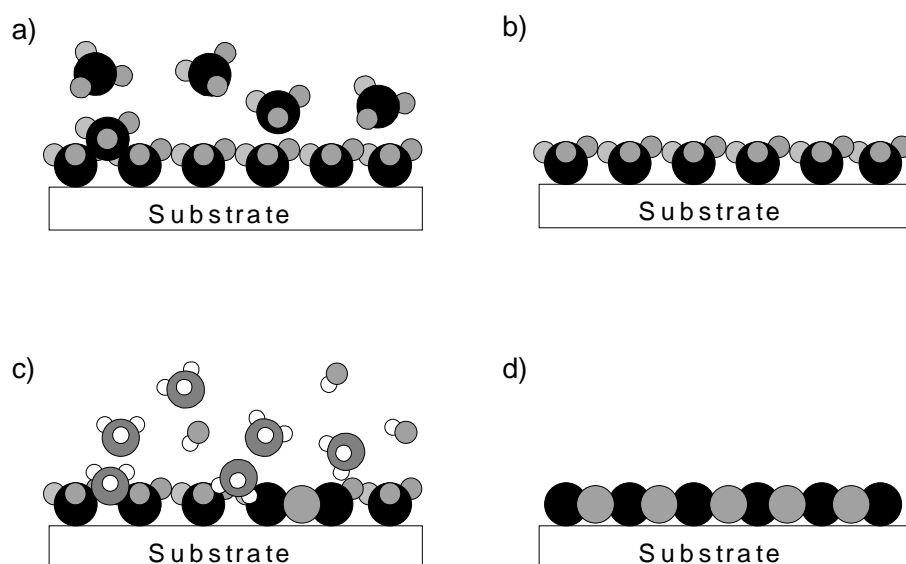


Figure 5.1. A schematic model of an ALD cycle. *a*) Chemisorption of the first precursor. *b*) One monolayer is adsorbed after purging. *c*) Introduction of the second precursor and subsequent surface reactions. *d*) The completion of one ALD cycle after the second purging.

By using the ALD method, materials of varying character like oxides, sulphides, nitrides, III-V compounds, II-VI compounds, and pure elements (e.g., Cu), have been deposited.^{4,5} The first report on ALD of a III-V material (GaAs) was published by Nishizawa *et al.* in 1985.⁶ Since then ALD has been used for several III-V compound semiconductors; AlN, GaN, GaP, InP, and InAs.⁷ The most common reactants for III-V nitrides are metal chlorides and metalorganic compounds as group III precursor, and ammonia as group V precursor.³

In the next section (5.3), the experimental details and the deposition of boron nitride from boron tribromide (BBr_3) and ammonia (NH_3) by means of ALD (**paper VII**) will be described.

5.3. Experimental details and results

Reactor design

The ALD experiments were carried out in a horizontal, hot-wall ALD reactor (Fig. 5.2). It consists of two tubes of fused silica (for spatial separation of the precursors before entering the reaction zone), a furnace, gas inlets for two reactant gases, reactor support and a substrate holder. Mass flow control units controlled the argon, nitrogen and ammonia gas flows. A constant flow through the mass flow control units was maintained by allowing the gases to be fed either into the reactor or in a by-pass line (to the pump). Air actuated valves controlled the direction (reactor or by-pass) of the different gas flows. The BBr_3 was allowed to diffuse into the reactor by its own vapour pressure and the flow rate was controlled by a needle valve. The regulation of pulse duration, pulse sequences and number of cycles was then computerised.

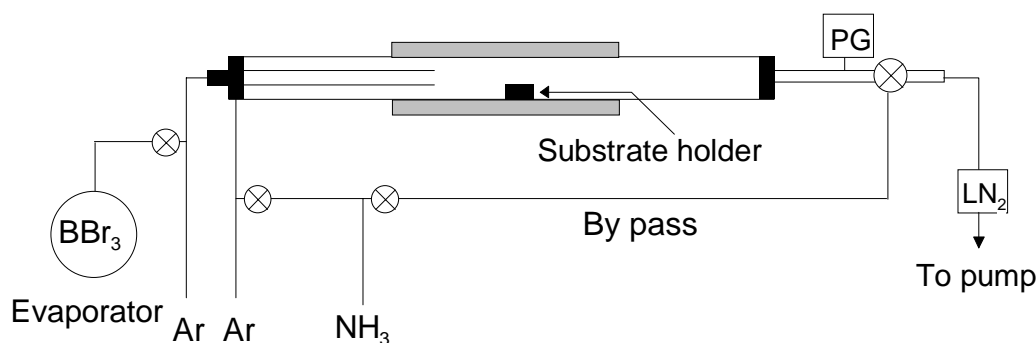


Figure 5.2. Horizontal hot-wall ALD system.

Film deposition

Thin films of boron nitride were deposited from boron tribromide (BBr_3) and ammonia (NH_3) by ALD in the reactor described above. The deposition temperatures were 400 and 750°C. The linear gas flow velocity was approximately 1 m/s, and the total pressure was 10 Torr in all experiments. The deposition parameters are presented in Table 2. As was mentioned in section 5.1, a gas phase chemistry consisting of mobile and less strongly surface-binding stabilisers (e.g., H) should be optimal in c-BN deposition. Thus, diborane (B_2H_6) and ammonia are the most obvious choices of precursors. However, since diborane is highly poisonous, boron tribromide was instead used as boron source. BBr_3 is a liquid with a high vapour pressure at room temperature (≈ 60 Torr).⁸ It reacts readily with ammonia, and from the periodicity of the boron trihalides it can be seen that BBr_3 is thermodynamically less stable (compared to BF_3 and BCl_3). This will lead to the formation of reactive B species at lower temperatures.⁹ Furthermore, the Br atoms are expected to be easily abstracted from the surface to leave room for incoming N-containing growth species.

Deposition temperature	400, 750°C
Total pressure	10 Torr
Linear gas velocity	1 m s ⁻¹
Typical pulse sequence (BBr -Ar-NH -Ar)	2-3-2-3 s
Number of cycles	500, 1000, 2000
Substrate	Silica

Table 2. Experimental parameters for the ALD deposition of boron nitride.

The influence of surface coverage of precursors (i.e., precursor saturation), number of cycles, and purge pulse length on the deposition rate was investigated through a series of experiments. By masking a minor part of the substrate, a step on the film surface was produced. Information about the film thickness was then obtained by measuring the height of the step using optical interferometry. The thickness could subsequently be related to the duration of the precursor pulses and purging pulse, as well as the number of cycles. It was found that, regardless of temperature or precursor, a maximum (or close to maximum) growth rate is obtained for a reaction pulse duration of 2 seconds. Furthermore, it has been found that at 400°C, the growth rate is almost constant regardless of purge pulse duration, whereas at 750°C, the growth rate is markedly decreasing as the duration of the purge pulse is increased (Fig. 5.3). This indicates that the different chemisorbed species are less strongly bonded to the surface at 750°C.

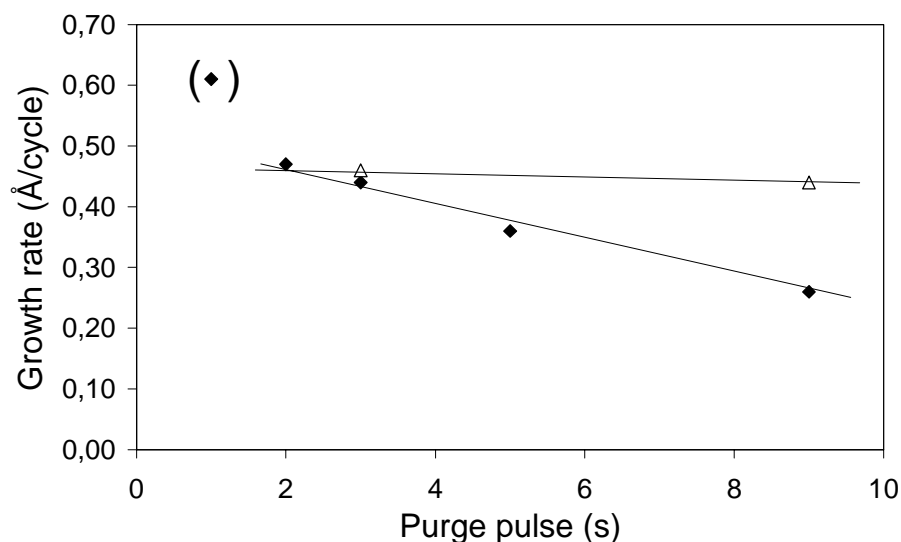


Figure 5.3. Growth rate as a function of the duration of the purge (Ar) pulse for 1000 cycles at (Δ) 400°C and (◆) 750°C. Reference lines are added to the diagram as a guide to the eye. The value at 1 second is omitted due to insufficient purging.

As mentioned earlier, one complete monolayer of the material should ideally be deposited in each ALD cycle. The average deposition rate for BN is 0.45 \AA/cycle , which means that it will require about 8 cycles to grow one monolayer of BN with the lattice spacing for the (002) plane being 3.33 \AA .¹⁰ However, by measuring the film thickness for 500, 1000 and 2000 cycles it can be found that the growth rate is linearly dependent on the number of cycles (Fig. 5.4). Thus, the deposition rate is constant throughout the process.

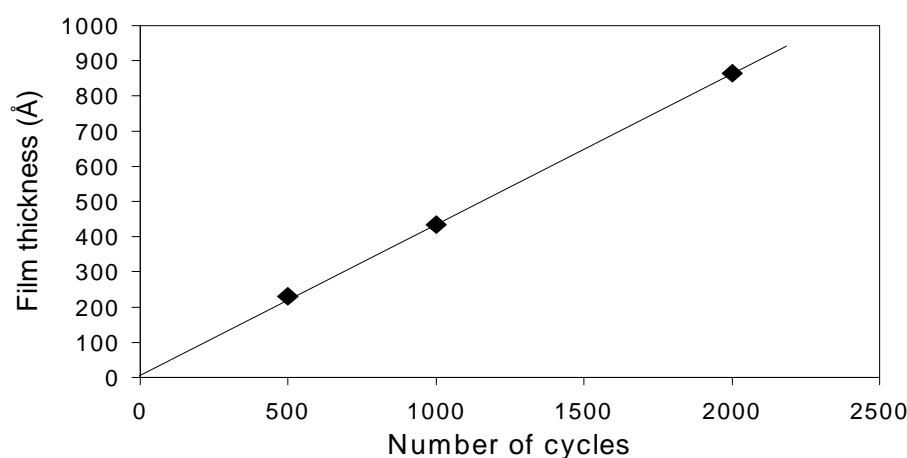


Figure 5.4. The film thickness of boron nitride as a function of the number of cycles at 750°C . The pulse sequence for these experiments is 2-3-2-3 s for BBr_3 , Ar, NH_3 and Ar, respectively.

Film characterisation

The BN films deposited by ALD are near-stoichiometric ($\text{B/N} \approx 0.95$), transparent and very smooth regardless of deposition temperature. The mean square surface roughness, measured by optical interferometry over a $1 \times 1\text{-}\mu\text{m}^2$ area, is $3\text{-}5 \text{ \AA}$. The observed lattice spacing of the h-BN (002) plane is 3.50 \AA for the deposited films (see below), which means that the surface roughness is approximately 1 monolayer.

The phase content was examined by means of X-ray Diffraction (XRD) (Grazing Incidence method (GI), $\text{CuK}\alpha$ radiation) and Micro-Raman spectroscopy ($\lambda = 785 \text{ nm}$). For the films deposited at 750°C , the X-ray diffractogram can be observed in Fig. 5.5. From the 2θ value of the h-BN (002) reflection, the c-axis is calculated to be 7.00 \AA , which indicates a turbostratic structure (t-BN).¹¹ The turbostratic structure is also confirmed with Raman spectroscopy. For the films deposited at 400°C , it was very difficult to obtain an X-ray diffractogram (within reasonable times), indicating that the films are less ordered than for a deposition temperature of 750°C . They may possibly even be amorphous.

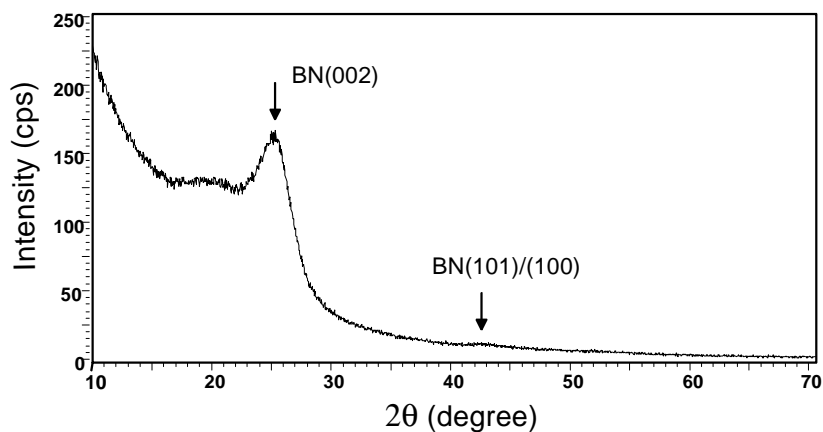


Figure 5.5. X-ray diffractogram (CuK α radiation) for boron nitride deposited on silica at 750°C.

The density of the films was measured by using the X-ray reflectometry method. It can be observed that the films grow denser as the temperature is increased from 400 to 750°C (ρ is calculated to be 1.65 – 1.70 vs. 1.90 – 1.95 g cm⁻³). This is an indication of the BN hexagonal layers becoming more ordered, which is also observed by XRD. The theoretical density for h-BN films is the bulk value of 2.27 g cm⁻³.¹²

It can be concluded that the films of boron nitride, deposited by ALD, are well-adherent and almost atomically smooth. With BN having a bandgap of at least 5 eV, the current process is a promising deposition method whenever thin insulating layers may be required. However, with an oxygen content in the films of $\approx 10\%$ at a deposition temperature of 400°C and $\approx 3\%$ at 750°C the process may need further development.

6. CONCLUDING REMARKS

Vapour phase deposition of a material open up many possibilities inaccessible for methods like sintering. Homogeneous reactions in the gas phase or on the surface, as well as heterogeneous reactions between species in the gas phase and species adsorbed on the growing surface, are processes that will provide the possibility of tailoring the deposition process. By acquiring knowledge of, and also controlling, the above reactions in connection to precursor design, the desired material, structure or phase may be deposited.

In this work, surface processes like adsorption, abstraction, migration and nucleation have been modelled on an atomic scale using density functional theory (DFT). The systems studied are mainly cubic and hexagonal boron nitride surfaces ((c-BN) vs. (h-BN)), but also the α -boron (001) surface.

It has been shown that modelling boron nitride with DFT requires the introduction of gradient-corrected functionals (BLYP or BP) to obtain reliable results. Furthermore, polarisation functions added to both hydrogen and heavier atoms are needed in the basis set for an adequate description of surface processes like adsorption of ammonia to h-BN (001). Two major approaches exist in modelling crystalline surfaces; either as a two-dimensional slab with periodic boundary conditions, or as a cluster. It was shown that the computationally less demanding model, the cluster, is a sufficient description of a crystalline BN surface. At least as long as constraints in the geometry optimisations are included.

A surface represents a violation of the three-dimensional symmetry found in the bulk. The boron and nitrogen atoms of c-BN are sp^3 -hybridised, meaning that on the different surfaces dangling bonds are present. These dangling bonds can either be terminated by different species, or cause the surface to reconstruct to an energetically more stable structure. It has been shown that an unterminated (111) surface will collapse and be subjected to graphitisation. By using H and F species to terminate the dangling bonds, the structure of the c-BN (111) surface, as well as the sp^3 -hybridisation of the surface B and N atoms was sustained. However, the F species were found to block the B (111) surface sites and thus most likely produce surfaces that are resistant to abstraction and to further growth of c-BN.

The nucleation of c-BN on both the basal plane and the basal plane edges, respectively, of h-BN (001) was investigated. It was observed that the B atoms in the basal plane would most probably have the capability to form embryonic c-BN nuclei (provided the gaseous environment is electron-rich, as in plasma or hot-filament CVD). Furthermore, the sp^3 character of these surface B atoms is decreasing when going from an electron-rich to an electron-deficient surface. On the other hand, the N

atoms of the h-BN basal plane were found to less likely participate in any formation of embryonic c-BN nuclei.

On the h-BN basal plane edges, it was shown that the cubic BN nuclei are significantly more stable than their hexagonal counterparts, regardless of whether the nuclei are derived from arbitrary or experimental growth species. This is especially the situation with F-terminated nuclei. Furthermore, the c-BN nucleation is energetically equally plausible in normal growth environments as in extremely radical-rich ones.

The chemical interaction of the diatomic molecules H_2 , Br_2 and HBr with α -boron (001) surfaces was investigated. Only the Br_2 and HBr molecules were demonstrated to adsorb dissociatively with the barrier of adsorption being too high for dissociation of H_2 . The Br species were found to exhibit a higher mobility than H species on the α -B surface. An Eley-Rideal type of abstraction mechanism (i.e., by gaseous species (here H or Br)) was energetically the most plausible for the adsorbed H or Br species.

Films of BN were deposited by atomic layer deposition (ALD). They showed a turbostratic structure (t-BN) when deposited at 750°C and were transparent, well-adherent and almost atomically smooth. With BN having a bandgap of at least 5 eV, the presented process is a promising deposition method whenever thin insulating layers may be required.

Conclusively, it has been theoretically shown that there may be gentle ways, using less brute force than PVD methods, to obtain thin films of cubic boron nitride. These ways would include surface stabilisers such as H species and a sequential deposition of alternating B- and N-containing species. The experimental part of the thesis showed evidence of a well functioning ALD process for BN thin films. However, with the cubic phase of boron nitride absent in the films, by means of this deposition process, more effort needs to be put into both the theoretical and the experimental branches of this field of science.

7. ACKNOWLEDGEMENT

First and foremost I would like to thank my supervisor Ass. Prof. Karin Larsson. I was your first full-time PhD student. Now, some five years later, your herd has increased and you've built yourself a small team. Not only did you in a good way guide me into the field of computational chemistry, but also, slowly and safely, you increased my responsibility regarding planning of projects, writing articles and rebutting and answering to referees' criticism. I now feel rather "self-consistent".

Secondly, Prof. Jan-Otto Carlsson is acknowledged for assigning me to this very interesting project and for putting all the equipment at the department at my disposal. I'm thankful, but honestly, to which PhD student haven't you done that? What I'm *personally* deeply and truly grateful for is that you gave me the opportunity to continue my "pentathletic" career. Without your help I could have kissed Atlanta goodbye already in December '95. But, alas, we now know the result. Never before has it been truer: Second place is the first loser!

The experimental part of this work would have been infinitesimally small without the enthusiastic and skilful help of Dr. Mikael Ottosson. Thank you for putting up with a theoretician. I think our theoretical/experimental blend made the whys and hows fall into place. What couldn't we have achieved with five more years?

Equally excellent and complementary practical help was obtained from Torvald, Janne and Anders. I'm still impressed how you turned my vague and virtual ideas into a live working apparatus. Keep it up, guys! Furthermore, Peter, Lillalars and JP are greatly acknowledged for invaluable help with the characterisation of the BN films.

Some people working silently in the background make life easier for the rest of us. Barbro, Dick, Gunilla and Ulrika, you're the grease in the machinery of our department. Without you: engine breakdown!

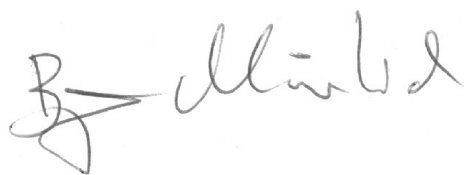
I would like to thank all past and present members of the inorganic family; Especially of the seniors, Anders E., "tant" Yvonne, Ingvar, Yngve "Orbital" and Anders H., who is greatly acknowledged for proof reading. Of the graduate students: Dr. Skåningen, the only one truly understanding me –from day one!

Names from the good old days at Kemikum; Leif Fornstedt, Kula, Sven Norén, Bettan, Hanna Bakfralla, Brigitte Bardot, Kristina, Maria, Åsa, Mankan, Per, Peo, Rikard, ... My under-grad years were some of the better ones. Full of memories for a nostalgian like me.

It's always difficult to express gratitude to the near ones, but Mor, Far, Magnus, Momme and unga-mormor Monica you've been a most essential real world support and connection. You've supplied me with the necessities of life: love, laughter and food. Furthermore, with one summerhouse on the West Coast and one on the East Coast, what more to ask for?

My wife Camilla and my children Tilde, Måns and "Plutten": You haven't directly contributed to the thesis, yet you are the most important. But, if it wasn't for you, this work might have been completed earlier, and the quality of it might even have been improved. Not that you ever hindered me from working, it was rather me struggling between the meaning of life and making a living. Life was boring when it was easy!

The Swedish Foundation for Strategic Research (SSF) and the Low-Temperature Thin Film Synthesis Program, the Swedish Natural Science Research Council (NFR), and the Swedish Research Council for Engineering Sciences (TFR) are acknowledged for financial support.

A handwritten signature in dark ink, appearing to read "Björn Almqvist". The signature is written in a cursive style with a large initial 'B' and a long horizontal stroke extending to the right.

Uppsala, April 2001

REFERENCES

Chapter 1, Introduction

1. L. Vel, G. Demazeau and J. Etourneau, *Mater. Sci. Eng. B* **10**, 149 (1991).
2. W. H. Balmain, *J. Prakt. Chem.* **27**, 422 (1842).
3. W. H. Balmain, *J. Prakt. Chem.* **32**, 494 (1844).
4. Carborundum Co., US Patent 2,808,314 (1957).
5. R. H. Wentorf Jr., *J. Chem. Phys.* **26**, 956 (1957).
6. V. N. Gashtol'd, S. A. Kutolin, L. M. Shakaryan, L. F. Belova and G. M. Komarova, *Elektron. Tekh. Ser.* **12**, 58 (1970).
7. K. Inagawa, K. Watanabe, H. Ohson, K. Saitoh and A. Itoh, *J. Vac. Sci. Technol. A* **5**, 2696 (1987).
8. J. Thomas Jr., N. E. Weston and T. E. O'Connor, *J. Am. Chem. Soc.* **84**, 4619 (1963).
9. F. P. Bundy and R. H. Wentorf Jr., *J. Chem. Phys.* **38**, 1144 (1963).
10. V. L. Solozhenko, *High Pressure Research* **13**, 199 (1995).
11. V. L. Solozhenko, *J. Hard Mater.* **6**, 51 (1995).
12. H. Sachdev, R. Haubner, H. Nöth and B. Lux, *Diam. Relat. Mater.* **6**, 286 (1997).
13. G. Will, G. Nover and J. v. d. Gönna, *J. Solid. Stat. Chem.* **154**, 280 (2000).
14. M. Z. Karim, D. C. Cameron and M. S. J. Hashmi, *Materials & Design* **13**, 207 (1992).
15. E. Yamaguchi, *Mater. Sci. Forum* **54-55**, 329 (1990).
16. S. P. S. Arya and A. D'Amico, *Thin Solid Films* **157**, 267 (1988).
17. G. Demazeau, *Diam. Relat. Mater.* **2**, 197 (1993).
18. R. Haubner and B. Lux, *Diam. Relat. Mater.* **2**, 1277 (1993).
19. I. Konyashin, J. Bill and F. Aldinger, *Chem. Vap. Deposition* **3**, 239 (1997).
20. T. Yoshida, *Diam. Relat. Mater.* **5**, 501 (1996).
21. W. Kulisch and S. Reinke, *Diam. Films Technol.* **7**, 105 (1997).
22. S. Reinke, M. Kuhr, W. Kulisch and R. Kassing, *Diam. Relat. Mater.* **4**, 272 (1995).
23. M. F. Plass, W. Fukarek, A. Kolitsch, N. Schell and W. Möller, *Thin Solid Films* **305**, 172 (1997).
24. D. J. Kester, K. S. Ailey, R. F. Davis and K. L. More, *J. Mater. Res.* **8**, 1213 (1993).
25. W. -L. Zhou, Y. Ikuhara, M. Murakawa, S. Watanabe and T. Suzuki, *Appl. Phys. Lett.* **66**, 2490 (1995).
26. M. J Rand and J. F Roberts, *J. Electrochem. Soc.* **115**, 423 (1968).
27. Y. Moriyoshi, S. Komatsu and T. Ishigaki, *Key Engineering Materials* **111-112**, 267 (1995).
28. W. Kulisch, R. Freudenstein, A. Klett and M. F. Plass, *Thin Solid Films* **377-378**, 170 (2000).

29. W. A. Yarbrough, *J. Vac. Sci. Technol. A* **9**, 1145 (1991).
30. A. Bartl, S. Bohr, R. Haubner and B. Lux, *Int. J. Ref. Metals Hard Mater.* **14**, 145 (1996).
31. I. Konyashin et al., *Chem. Vap. Deposition* **4**, 125 (1998).
32. P. B. Mirkarimi et al., *J. Mater. Res.* **9**, 2925 (1994).
33. T. Ichiki, S. Amagi and T. Yoshida, *J. Appl. Phys.* **79**, 4381 (1996).
34. J. Robertson, *Diam. Relat. Mater.* **5**, 519 (1996).
35. K. F. McCarty, P. B. Mirkarimi, D. L. Medlin, T. A. Friedmann and J. C. Barbour, *Diam. Relat. Mater.* **5**, 1519 (1996).
36. Y. Bar-Yam, T. Lei, T. D. Moustakas, D.C. Allan and M. P. Teter, *Mater. Res. Soc. Symp. Proc.* **242**, 335 (1992).
37. S. Bohr, R. Haubner and B. Lux, *Diam. Relat. Mater.* **4**, 714 (1995).
38. R. M. Desrosiers, D. W. Greve and A. J. Gellman, *Surf. Sci.* **382**, 35 (1997).
39. S. Middleman, *Mater. Sci. Eng. A* **163**, 135 (1993).
40. A. H. McDaniel and M.D. Allendorf, *J. Phys. Chem. A* **102**, 7804 (1998).
41. M. D. Allendorf, C. F. Melius and T. H. Osterheld, *Mater. Res. Soc. Symp. Proc.* **410**, 459 (1996).

Chapter 2, Density Functional Theory (DFT)

1. J. Almlöf, K. Faegri and K. Korsell, *J. Comput. Chem.* **3**, 385 (1982).
2. W. Klopper and W. Kutzelnigg, *J. Chem. Phys.* **94**, 2020 (1991).
3. R. E. Stratmann, G. E. Scuseria and M. J. Frisch, *Chem. Phys. Lett.* **257**, 213 (1996).
4. E. Fermi, *Rend. Accad., Lincei* **6**, 602 (1927).
5. E. Fermi, *Z. Phys.* **48**, 73 (1928).
6. L. H. Thomas, *Proc. Camb. Phil. Soc.* **23**, 542 (1927).
7. J. C. Slater, *Phys. Rev.* **81**, 385 (1951).
8. P. A. M. Dirac, *Proc. Cambridge Philos. Soc.* **26**, 376 (1930).
9. E. Teller, *Rev. Mod. Phys.* **34**, 627 (1962).
10. P. Hohenberg and W. Kohn, *Phys. Rev. B* **136**, 864 (1964).
11. E. B. Wilson, in *Structural Chemistry and Biology*, W. H. Freeman (San Francisco), 753-760 (1968).
12. R. G. Parr and W. Yang, in *Density Functional Theory*, Oxford University Press (Oxford) (1989).
13. W. Kohn and L. J. Sham, *Phys. Rev. A* **140**, 1133 (1965).
14. T. Koopmans, *Physica* **1**, 104 (1934).
15. P. Politzer and F. Abu-Awwad, *Theor. Chem. Acta* **99**, 83 (1998).
16. A. Zangwill, in *Physics at Surfaces*, Cambridge University Press (Cambridge) (1988).
17. D. M. Ceperley and B. J. Alder, *Phys. Rev. Lett.* **45**, 566 (1980).
18. S. J. Vosko, L. Wilk and M. Nusair, *Can. J. Phys.* **58**, 1200 (1980).
19. R. G. Parr and W. Yang, in *Density Functional Theory*, Oxford University Press (Oxford), Appendix E (1989).

20. R. O. Jones and O Gunnarsson, *Reviews of Modern Physics* **60**, 689 (1989).
21. U. von Barth, *Chemica Scripta* **26**, 449 (1986).
22. L. A. Curtiss, K Raghavachari, P. C. Redfern and J. A. Pople, *J. Chem. Phys.* **106**, 1063 (1997).
23. J. P. Perdew, *Phys. Rev. B* **33**, 8822 (1986).
24. J. P. Perdew, J. A. Chevary, S. H. Vosko, K. A. Jackson, M. R. Pederson, D. J. Singh and C. Fiolhais, *Phys. Rev. B* **46**, 6671 (1992).
25. A. D. Becke, *J. Chem. Phys.* **88**, 2547 (1988).
26. G. Ortiz and P Ballone, *Phys. Rev. B* **43**, 6376 (1991).
27. R. Colle and O. Salvetti, *Theor. Chem. Acc.* **37**, 329 (1975).
28. C. Lee, W. Yang and R. G. Parr, *Phys. Rev. B* **37**, 785 (1988).
29. A. D. Becke, *J. Chem. Phys.* **98**, 1372 (1992).
30. A. D. Becke, *J. Chem. Phys.* **98**, 5648 (1993).

Chapter 3, DFT reliability in boron nitride modelling

1. B. Delley, *J. Chem. Phys.* **92**, 508 (1990).
2. P. Hohenberg and W. Kohn, *Phys. Rev. B* **136**, 864 (1964).
3. W. Kohn and L. J. Sham, *Phys. Rev. A* **140**, 1133 (1965).
4. U. von Barth and L. Hedin, *J. Phys. C* **5**, 1629 (1972).
5. L. Hedin and B. I. Lundqvist, *J. Phys. C* **4**, 2064 (1971).
6. J. F. Janak, V. L. Moruzzi and A. R. Williams, *Phys. Rev. B* **12**, 1257 (1975).
7. S. J. Vosko, L. Wilk and M. Nusair, *Can. J. Phys.* **58**, 1200 (1980).
8. J. P. Perdew, *Phys. Rev. B* **33**, 8822 (1986).
9. P. A. M. Dirac, *Proc. Camb. Phil. Soc.* **26**, 376 (1930).
10. A. D. Becke, *J. Chem. Phys.* **88**, 2547 (1988).
11. C. Lee, W. Yang and R. G. Parr, *Phys. Rev. B* **37**, 785 (1988).
12. J. P. Perdew, J. A. Chevary, S. H. Vosko, K. A. Jackson, M. R. Pederson, D. J. Singh and C. Fiolhais, *Phys. Rev. B* **46**, 6671 (1992).
13. A. G. Gaydon in *Dissociation Energies and Spectra of Diatomic Molecules* (Chapman and Hall, London, 1968).
14. I. Konyashin, J. Bill and F. Aldinger, *Chem. Vap. Deposition* **3**, 239 (1997).
15. M. F. Plass, W. Fukarek, A. Kolitsch, N. Schell and W. Möller, *Thin Solid Films* **305**, 172 (1997).
16. W. -L. Zhou, Y. Ikuhara, M. Murakawa, S. Watanabe and T. Suzuki, *Appl. Phys. Lett.* **66**, 2490 (1995).
17. P. Widmayer, H. -G. Boyen, P. Ziemann, P. Reinke and P. Oelhafen, *Phys. Rev. B* **59**, 5233 (1999).
18. L. A. Curtiss, K. Raghavachari, P. C. Redfern and J. A. Pople, *J. Chem. Phys.* **106**, 1063 (1997).
19. A. D. Becke, *J. Chem. Phys.* **97**, 9173 (1992).
20. H. Nakai, T. Goto, T. Ichikawa, Y. Okada, T. Orii and K. Takeuchi, *Chem. Phys.* **262**, 201 (2000).
21. B. G. Johnson, P. M. W. Gill and J. A. Pople, *J. Chem. Phys.* **98**, 5612 (1993).

22. C. W. Murray, G. J. Laming, N. C. Handy and R. D. Amos, *Chem. Phys. Lett.* **199**, 551 (1992).
23. *DMol User Guide*, version 2.3.0.; Biosym Technologies: San Diego, 1993.
24. S. F. Boys and F. Bernardi, *Mol. Phys.* **19**, 553 (1970).
25. D. W. Schwenke and D. G. Truhlar, *J. Chem. Phys.* **82**, 2418 (1985).
26. M. Alfredsson, L. Ojamäe and K. Hermansson, *Int. J. Quant. Chem.* **60**, 767 (1996).
27. B. Civalleri, E. Garrone and P. Ugliengo, *J. Mol. Struct. (Theochem)* **419**, 227 (1997).
28. G. Fitzgerald and J. Andzelm, *J. Phys. Chem.* **95**, 10531 (1991).
29. J. M. Seminario, *Chem. Phys. Lett.* **206**, 547 (1993).
30. J. Amorim, A. G. Baravian and G. Sultan, *Appl. Phys. Lett.* **68**, 1915 (1996).
31. J. L. Durant, *Chem. Phys. Lett.* **256**, 595 (1996).
32. R. H. Hertwig and W. Koch, *J. Comp. Chem.* **16**, 576 (1995).
33. R. J. D. Miller, G. L. McLendon, A. J. Nozik, W. Schmickler and F. Willig, in *Surface Electron Transfer Processes* (VCH Publishers, New York, 1995).
34. E. Yamaguchi, *Mater. Sci. Forum* **54-55**, 329 (1990).
35. R. M. Chrenko, *Solid State Comm.* **14**, 511 (1974).
36. J. P. Perdew and Y. Wang, *Phys. Rev. B* **45**, 13244 (1992).
37. J. P. Perdew and A. Zunger, *Phys. Rev. B* **23**, 5048 (1981).
38. K. Larsson and J. -O. Carlsson, *J. Phys. Chem. B* **103**, 6533 (1999).

Chapter 4, Results

1. D. Huang, M. Frenklach and M. Maroncelli, *J. Phys. Chem.* **92**, 6379 (1988).
2. M. Frenklach and K. Spear, *J. Mater. Res.* **3**, 133 (1988).
3. J. Widany, F. Weich, Th. Köhler, D. Porezag and Th. Frauenheim, *Diam. Rel. Mater.* **5**, 1031 (1996).
4. P. Widmayer, H. -G. Boyen, P. Ziemann, P. Reinke and P. Oelhafen, *Phys. Rev. B* **59**, 5233 (1999).
5. L. Vel, G. Demazeau and J. Etourneau, *Mater. Sci. Eng. B* **10**, 149 (1991).
6. R. I. Morrison and R. N. Boyd, in *Organic Chemistry* (Allyn and Bacon, Boston, 1973).
7. K. Spear, *J. Am. Ceram. Soc.* **72**, 171 (1989).
8. A. Badzian and R. DeVries, *Mater. Res. Bull.* **23**, 385 (1988).
9. W. J. Zhang and S. Matsumoto, *Chem. Phys. Lett.* **330**, 243 (2000).
10. S. Bohr, R. Haubner and B. Lux, *Diam. Relat. Mater.* **4**, 714 (1995).
11. K. Larsson and J. -O. Carlsson, *J. Phys. Chem. B* **103**, 6533 (1999).
12. A. Lindlbauer, R. Haubner and B. Lux, *Wear* **159**, 67 (1992).
13. K. P. Loh, I. Sakaguchi, M. Nishitano-Gamo, T. Taniguchi and T. Ando, *Phys. Rev. B* **57**, 7266 (1998).
14. I. Konyashin et al., *Thin Solid Films* **355-356**, 96 (1999).
15. V. Khvostov, I. Konyashin, E. Shouleshev, V. Babaev and M. Guseva, *Appl. Surf. Sci.* **157**, 178 (2000).

16. M. F. Plass, W. Fukarek, A. Kolitsch, N. Schell and W. Möller, *Thin Solid Films* **305**, 172 (1997).
17. D. R. McKenzie et al., *J. Appl. Phys.* **70**, 3007 (1991).
18. T. A. Friedmann et al., *J. Appl. Phys.* **76**, 3088 (1994).
19. C. A. Taylor II and R. Clarke, *Mater. Res. Soc. Symp. Proc.* **423**, 265 (1996).
20. D. R. McKenzie, W. D. Fall, W. G. Sainty, C. A. Davis and R. E. Collins, *Diam. Relat. Mater.* **2**, 970 (1993).
21. R. Riedel, *Adv. Mater.* **6**, 549 (1994).
22. M. Terrones et al., *Chem. Phys. Lett.* **257**, 576 (1996).
23. O. Stephan, P. M. Ajayan, C. Colliex, P. Redlich, J. M. Lambert and P. Bernier, *Science* **266**, 1683 (1994).
24. H. F. Zhang, C. Y. Wang, W. H. Duan and R. C. Fang, *Defect and Diffusion Forum* **152**, 19 (1997).
25. I. Konyashin, V. Khvostov, V. Babaev, M. Guseva, J. Bill and F. Aldinger, *Diam. Relat. Mater.* **8**, 2053 (1999).
26. J. Widany, T. Frauenheim and W. R. L. Lambrecht, *J. Mater. Chem.* **6**, 899 (1996).
27. S. P. Mehandru, A. B. Andersson and J. C. Angus, *J. Phys. Chem.* **96**, 10978 (1992).
28. A. H. McDaniel and M.D. Allendorf, *J. Phys. Chem. A* **102**, 7804 (1998).
29. I. Konyashin, J. Bill and F. Aldinger, *Chem. Vap. Deposition* **3**, 239 (1997).
30. C. Zirc and R. Ahlrichs, *J. Chem. Phys.* **75**, 4980 (1981).
31. J. S. Binkley and L. R. Thorne, *J. Chem. Phys.* **79**, 2932 (1983).
32. T. Brink, J. S. Murray and P. Politzer, *Inorg. Chem.* **32**, 2622 (1993).
33. V. Jonas, G. Frenking and M. T. Reetz, *J. Am. Chem. Soc.* **116**, 8741 (1994).
34. H. W. Kroto and D. McNaughton, *J. Chem. Soc., Dalton Trans.* **9**, 1767 (1985).
35. A. C. Legon and H. E. Warner, *J. Chem. Soc., Chem. Commun.* **19**, 1397 (1991).
36. A. G. Avent et al., *J. Chem. Soc., Chem. Commun.* **8**, 855 (1995).
37. M. D. Allendorf and C. F. Melius, *J. Phys. Chem. A* **101**, 2670 (1997).
38. M. D. Allendorf and C. F. Melius, *Surf. Coat. Technol.* **108-109**, 191 (1998).
39. I. Konyashin, J. Loeffler, J. Bill and F. Aldinger, *Thin Solid Films* **308-309**, 101 (1997).
40. I. Konyashin et al., *Thin Solid Films* **355-356**, 96 (1999).
41. S. Komatsu, W. Yarbrough and Y. Moriyoshi, *J. Appl. Phys.* **81**, 7798 (1997).
42. M. Carbone, K. Larsson and J. -O. Carlsson, *J. Phys. Chem. A* **101**, 9445 (1997).
43. M. Carbone, K. Larsson and J. -O. Carlsson, *J. Phys. Chem. B* **102**, 5866 (1998).
44. D. W. Bullett, *J. Phys. C* **15**, 415 (1982).
45. E. Yamaguchi, *Mater. Sci. Forum* **54-55**, 329 (1990).
46. W. Klein, *J. Less-Common Met.* **47**, 101 (1976).
47. J. -O. Carlsson, *J. Less-Common Metals* **71**, 1 (1980).
48. E. A. Haupfear and L. D. Schmidt, *Chem. Eng. Sci.* **49**, 2467 (1994).
49. N. A. Sezgi, T. Dogu and H. O. Ozbelge, *Ind. Eng. Chem. Res.* **36**, 5537 (1997).
50. I. A. Howard and A. K. Ray, *Phys. Rev. B* **45**, 3680 (1992).
51. B. Sykja and S. Lunell, *Surf. Sci.* **141**, 199 (1984).
52. B. F. Decker and J. S. Kasper, *Acta Cryst.* **12**, 503 (1959).
53. J. -O. Carlsson, *J. Less-Common Metals* **70**, 77 (1980).

54. J. A. Ugai and N. E. Soloviev, in *Boron and Refractory Borides* (Springer Verlag, Berlin, 1977).
55. I. Langmuir, *Trans. Faraday Soc.* **17**, 621 (1922).
56. T. Sekine, N. Nakanishi and E. Kato, *J. Jpn. Inst. Met.* **53**, 698 (1989).
57. D. D. Eley, *Chem. Ind.* **1976(1)**, 12 (1976).

Chapter 5, ALD of boron nitride

1. K. Larsson and J. –O. Carlsson, *J. Phys. Chem. B* **103**, 6533 (1999).
2. T. Suntola and J. Antson, *US Patent* 4,058,430 (1977).
3. M. Leskelä and M. Ritala, *J. Phys. IV C5*, 937 (1995).
4. T. Suntola and M. Simpson (Eds.), in *Atomic Layer Epitaxy*, Blackie and Son Ltd (Glasgow) (1990).
5. P. Mårtensson and J. –O. Carlsson, *Chem. Vap. Deposition* **3**, 45 (1997).
6. J. Nishizawa, H. Abe and T. Kurabayashi, *J. Electrochem. Soc.* **132**, 1197 (1985).
7. A. Usui, *Proc. IEEE* **80(10)**, 1641 (1992).
8. Gmelin Handbuch der anorganischen Chemie 13, 8. Auflage, Verlag Chemie, Leipzig-Berlin, 1926.
9. R. Naslain, J. Thebault and P. Hagenmuller, *J. Less-Common Met.* **67**, 85 (1979).
10. R. S. Pease, *Acta Cryst.* **5**, 356 (1952).
11. J. Thomas Jr., N. E. Weston and T. E. O'Connor, *J. Am. Chem. Soc.* **84**, 4619 (1963).
12. A. Lipp, K. A. Schwetz and K. Hunold, *J. Eur. Ceram. Soc.* **5**, 3 (1989).

Illustration on front cover:

Control of reaction pathways during growth of advanced materials using density functional theory calculations and molecular dynamics simulation.
Courtesy of Karin Larsson.